REVIEWS OF TOPICAL PROBLEMS

Nonequilibrium phase transformations in alloys under severe plastic deformation

Physics – Uspekhi **63** (8) 733 – 757 (2020)

REVIEWS OF TOPICAL PROBLEMS

PACS numbers: 61.50.Ks, 62.20.F –, 64.60.Cn, 64.70.K –

Nonequilibrium phase transformations in alloys under severe plastic deformation

I K Razumov, A Y Yermakov, Yu N Gornostyrev, B B Straumal

DOI: https://doi.org/10.3367/UFNe.2019.10.038671

Contents

1. Introduction **733**
2. Scenarios and mechanisms of phase transformations in alloys subjected to severe plastic deformation **734**
2.1 Stationary state under severe plastic deformation; 2.2 Disordering and amorphization of alloys; 2.3 Formation of supersaturated solid solutions and highly dispersed states; 2.4 Abnormal decomposition of alloys and compounds, cyclic reactions
3. Segregations and grain-boundary decomposition in nanocrystalline materials **745**
4. Problem of abnormal diffusion under intense plastic deformation **748**
5. Classification of phase transformations under severe plastic deformation **750**
6. Conclusion **753**
References **753**

Abstract. Experimental results and theoretical concepts of anomalous phase transformations in alloys under severe plastic deformation (SPD) are reviewed. The unconventional phase and structural state of alloys that emerges as a result of SPD determines the unique combination of physical and chemical properties that is of interest for various applications in technology. The driving forces and possible mechanisms that implement the anomalous transformations as a function of SPD intensity, alloy composition, and temperature are discussed. We distinguish among these mechanisms two fundamental and qualitatively different ones that are due to: (i) direct 'mixing' of atoms in slip bands or (ii) accelerated diffusion on defects under locally alternating thermodynamic conditions and subsequent 'freezing' of the nonequilibrium state that is reached. Summarizing the experimental data and theoretical concepts regarding the change in microscopic transformation mechanisms as a function of temperature and/or intensity of treatment, we suggest a diagram of nonequilibrium stationary states attainable during the development of phase and structural instability under SPD. The proposed approach enables the prediction of the structural state of alloys and compounds by controlling thermodynamic and kinetic parameters of the system.

Keywords: severe plastic deformation, mechanical alloying, disordering, amorphization, grain boundary segregation, mechanical mixing

I K Razumov [(1, a)], **A Y Yermakov** [(1, 2, b)], **Yu N Gornostyrev** [(1, 2, 3, c)], **B B Straumal** [(4, 5, 6, d)]
[(1)] Mikheev Institute of Metal Physics, Ural Branch of the Russian Academy of Sciences, ul. S Kovalevskoi 18, 620108 Ekaterinburg, Russian Federation
[(2)] Ural Federal University named after the First President of the Russian Federation, B N Yeltsin, ul. Mira 19, 620002 Ekaterinburg, Russian Federation
[(3)] Institute of Quantum Materials Science, ul. Konstruktorov 5, 620007 Ekaterinburg, Russian Federation
[(4)] Institute of Solid State Physics, Russian Academy of Sciences, ul. Akademika Osip'yana 2, 142432 Chernogolovka, Moscow region, Russian Federation
[(5)] Scientific Center Chernogolovka, Russian Academy of Sciences, ul. Lesnaya 9, 142432 Chernogolovka, Moscow region, Russian Federation
[(6)] National University of Science and Technology MISiS, Leninskii prosp. 4, 119049 Moscow, Russian Federation
E-mail: [(a)] rik@imp.uran.ru, [(b)] yermakov@imp.uran.ru, [(c)] yug@imp.uran.ru, [(d)] straumal@issp.ac.ru

Received 6 May 2019
Uspekhi Fizicheskikh Nauk **190** (8) 785 – 810 (2020)
Translated by M Zh Shmatikov; edited by V L Derbov

1. Introduction

Severe plastic deformation (SPD) is an efficient technique to obtain nanocrystalline materials with a grain size of 100–300 nm in pure metals and less than 20 nm in alloys [1–4], along with a unique combination of physicochemical properties. Increased attention has been drawn in recent decades to unconventional solid-phase transformations and structural states, which occur under severe deformation or subsequent heat treatment. They include disordering [5–10] and amorphization [8, 9, 11–19], a reduction in oxides up to pure metals [20, 21], the formation of solid solutions in systems with negative [9, 22] and positive enthalpy of mixing (anomalous mechanical alloying) [13, 23–27], the competition between formation and decomposition of solid solutions with a transition to a stationary dispersed state [28–30], the dissolution of particles of intermetallics [31, 32], oxides [33–35], carbides [36, 37], and nitrides [38, 39] in steels and alloys, a rapid realization of low-temperature equilibrium or metastable phases [40–43], the formation of wide grain-boundary segregations [44–48] and grain-boundary layers [49], abnormal decomposition with the formation of nonequilibrium

phases [50–52], and amorphization/nanocrystallization or decomposition/mixing cyclic reactions [53, 54]. The attained state of the alloy is 'frozen' after the termination of the external influence, which determines the technological attractiveness of this method for processing materials.

A deep understanding of the processes that develop under SPD is of great practical importance. For example, the idea to enhance the hysteresis properties of permanent magnets based on 4f-3d-metals by means of mechanical activation turned out to be invalid, since alloys undergo a crystal-amorphous state phase transition before a high-coercive state is attained [11, 12]. Similar phase transitions are observed in the process of mechanical activation in exchange-enhanced systems, which are a mixture of soft magnetic phases and a highly anisotropic component. Subsequent annealing that partially restores the structure may further enhance the undesired decomposition of the system, thus degrading the properties of both single-phase and exchange-enhanced permanent magnets. Thus, the phase instability of the system is a factor that controls its physical properties.

The materials obtained using SPD techniques feature high strength, corrosion and radiation resistance, and special electrical and magnetic properties (for example, Co_2Ge and $GdAl_2$ ferromagnetic alloys transform from an amorphous state into spin glasses) [9, 55, 56]. Dispersion-hardening alloys based on iron, nickel, and aluminum, which are obtained by mechanical alloying, are applied in aerospace technologies (turbine blades, combustion chambers) owing to their high corrosion resistance and hardening effect due to the presence of dispersed oxide precipitates [13]. Mg–Fe (Cu, Cr) alloys obtained by mechanical alloying are widely used as fuel cells owing to the high reaction rate upon contact with an electrolyte (such as sea water) [13]. Structural changes that occur in the process of mechanosynthesis also significantly affect the biopharmaceutical properties of manufactured drugs, such as solubility, hygroscopicity, and, in certain cases, their toxicity [57].

Despite the large number of studies, a comprehensive understanding of phase and structural transformations under SPD is still lacking. There is no doubt that a prerequisite for the development of abnormal transformations is a certain intensity of external deformation, which is usually accompanied by a refinement of the structure and a transition to a nanograin state. However, the specific mechanisms that determine the formation of the phase and structural state under SPD conditions or subsequent annealing are a matter of discussion. For example, anomalous mechanical alloying in systems that are thermodynamically prone to decomposition (Fe–Cu, Cu–Co, Fe–Pb, etc.) is explained by direct mixing due to shears in intersecting planes [58, 59], the interaction of precipitates with dislocations [32, 60, 61], dissolution of subcritical precipitates in the process of grinding grains [26], and a shift of the phase diagram to the high-temperature region due to the accumulation of defects [62]. Therefore, classification of abnormal transformations under SPD and identification of the conditions, driving forces, and microscopic mechanisms of their implementation remain relevant issues.

We analyze in this review accumulated experimental data to show that the concepts based on the mechanism of direct mechanical mixing of atoms are insufficient to explain the entire set of facts concerning the development of phase transformations under SPD. Mass transport in the region of crystal lattice defects (dislocations and grain boundaries) can play a decisive role at moderate temperatures in the development of phase transformations. A transformation (for example, disordering or dissolution of precipitates) occurs in this case locally in the region of a structural defect, under altered thermodynamic conditions (compared to those in the bulk), and the attained state is frozen after the displacement of the defect due to the low rate of bulk diffusion. The alloy can, as a result, move away from thermodynamic equilibrium, even in the absence of mechanical mixing.

Based on an analysis of experimental data and existing concepts, we propose considering the formation of nonequilibrium states of the alloy as a result of dissipation of the supplied mechanical energy through an available channel (diffusion redistribution of alloy components, slip of dislocations, refinement of the grain structure, low-temperature dynamic recrystallization, etc.), the implementation of which depends on temperature and intensity of processing. Direct mixing prevails at low temperatures and intense plastic deformation, which leads to amorphization and mechanical alloying. At high temperatures and weak deformation, bulk diffusion facilitates the formation of equilibrium phases. In processing at moderate temperatures, nonequilibrium transformations may occur due to accelerated mass transport along dislocations and grain boundaries under conditions of frozen bulk diffusion.

A conceptual basis arises as a result for the classification of abnormal phase transformations in the temperature-intensity coordinates, which is based on the general principles of nonequilibrium thermodynamics. This allows an explanation from a unified standpoint of a large set of experimental observations and the prediction of the mechanism that drives development of phase or structural instability of an alloy under SPD with relevant relaxation mechanisms taken into account.

2. Scenarios and mechanisms of phase transformations in alloys subjected to severe plastic deformation

The variety of structural and phase transformations observed under severe deformation is due to the significant dependence of the evolution of the system, which is far from the equilibrium state, on external conditions. Many authors note the qualitative similarity between transformations that occur under SPD and irradiation [14, 32, 63]. However, the processes that occur under SPD have their own specifics and are less studied. As the intensity of the deformation increases, the average grain size decreases, and the dislocation deformation mode is replaced by the rotational mode [64], which, in the opinion of the authors of [65], also degenerates when the grain size attains ~ 200 nm. The decisive role is played in the nanocrystalline state by processes that occur in the region of grain boundaries (grain boundary diffusion and the formation of segregations [66], grain boundary sliding [67], low-temperature dynamic recrystallization [65]), the structure of grain boundaries being strongly distorted (nonequilibrium) [3]. SPD leads also to an intense generation of point defects (vacancies and interstitial atoms [68, 69]). The concentration of vacancies attains in this case pre-melting values ($\sim 10^{-4}$) [70–74], enabling diffusion even at low temperatures.

2.1 Stationary state under severe plastic deformation

An important feature of SPD is that the sample cannot be destroyed in the process of deformation, and its shape remains more or less unchanged. This is especially true in

the case of high-pressure torsion (HPT). The small disc between two anvils retains its shape, regardless of the number of revolutions of anvils. While the anvils withstand about 20 revolutions under HPT of Nd–Fe–B alloys [75, 76], in the case of soft alloys based on aluminum or copper, HPT can last up to several hundred or even thousands of revolutions of the anvils [77–80]. The number of lattice defects (vacancies, dislocations, grain boundaries) increases as expected in the course of deformation. However, this process does not develop at a constant rate with multiple revolutions of the anvils. Relaxation begins even if SPD occurs at room temperature when the bulk diffusion coefficients do not exceed $10^{-30}-10^{-40}$ m^2 s^{-1}. (It should be noted that SPD usually occurs just at room temperature, and samples hardly heat up during processing [81, 82]: direct measurements show that the sample temperature during HPT does not exceed 40 °C [83, 84].) The rate of relaxation (annihilation) of defects increases as their concentration grows, until a steady state is attained, at which the rate of defect formation is equal to the rate of their annihilation [85, 86]. The easiest way to observe the onset of the steady state is to measure the torsion torque during HPT. It increases during the transient stage, but is quickly saturated after 1–1.5 revolutions for alloys based on aluminum, copper, or even titanium [83, 85, 87, 88]. In the case of harder alloys, such as Nd–Fe–B, the torsion torque stops increasing after 2–2.5 anvil revolutions [75, 76, 85].

Apart from the torsion torque, other physical properties or structural parameters are saturated at the steady state. Thus, under deformation of a material with a grain size of several millimeters, the grains are rapidly refined to several hundred nanometers [2, 89–91], and, if deformation continues, their size attains a steady-state value [86, 92–95], which depends on the SPD regime. The smallest grain size in copper and copper-based alloys, about 15 nm, is attained by grinding in a ball mill (Fig. 1) [96]. The second most efficient method of grain refinement is HPT [87, 97–102]. This is followed by planar twist channel angular extrusion (PTCAE) [103], equal channel angular pressing (ECAP) [100, 104], ECAP followed by HPT (ECAP + HPT) [100], ECAP followed by the cold rolling (ECAP + CR) [105], simple shear extrusion (SSE) [106,107], and the constrained groove pressing (CGP) [108].

The same trend is typical of aluminum and its alloys [109]. The stationary grain size also depends on pressure, strain rate, and HPT temperature [85, 86]. It decreases with an increase in the melting temperature, atomic bond energy, specific heat, and self-diffusion activation energy [86, 110]. It should be emphasized that the stationary grain size may be attained not only 'from above' but also 'from below'. For example, the grain size quickly attains 15–20 nm under HPT of coarse-grained steel [94, 111–117] (Fig. 2). If a sample of nanocrystalline steel with a grain size of 10 nm, which is obtained by mechanical alloying, is deformed, the grains do not decrease, but increase under SPD to attain the same stationary value of 15–20 nm (see Fig. 2) [77]. A similar phenomenon has been observed in nickel [118, 119].

There is a large amount of data on Vickers microhardness during and after SPD for steels and alloys of aluminum, titanium, and magnesium [78, 84, 95, 120–132]. Typically, the microhardness increases during SPD [78, 84, 95, 120–132], which correlates with tensile strength [122, 125]. This is true for both the rotation angle at HPT and the number of ECAP passes [127]. The main mechanism here is Hall–Petch hardening due to grain refinement [133]. The few exceptions only confirm this conclusion. For example, Hall–Petch hardening competes in Al–Zn alloys with the softening caused by the decomposition of the solid solution (Al), as a result of which the alloy becomes softer after HPT than prior to it [97, 121, 134, 135]. Similar to the grain size, hardness is also a function of the material and SPD regime. For example, if the purity of aluminum is increased, a transition from hardening to softening is observed under HPT [136], i.e., if the initial hardness of the alloy is higher than the stationary value, softening rather than strain-hardening is observed under SPD [134].

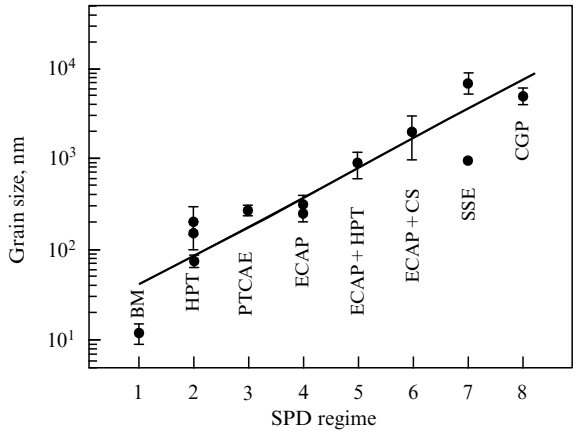

Figure 1. Stationary grain size in copper under various SPD modes: 1 — ball milling (BM) [96], 2 — high pressure torsion (HPT) [87, 97–102], 3 — planar twist channel angular extrusion (PTCAE) [103], 4 — equal channel angular pressing (ECAP) [100, 104], 5 — ECAP + HPT [100], 6 — equal-channel angular extrusion followed by cold rolling (ECAP + CR) [105], 7 — simple shear extrusion (SSE) [106, 107], 8 — constrained groove pressing (CGP) [108].

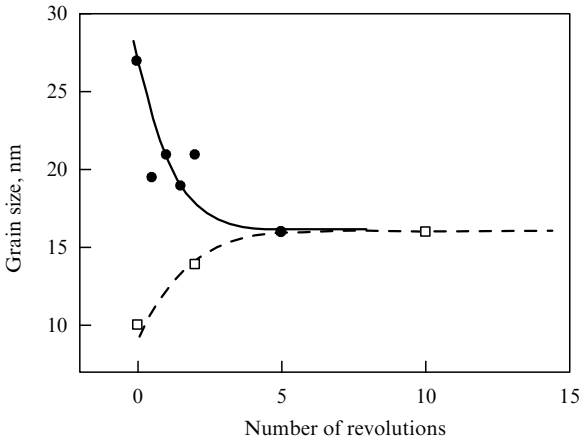

Figure 2. Grain size as a function of the number of revolutions of the anvils for a sample of pure coarse-grained steel (dots) [112] and nanocrystalline steel obtained by mechanical alloying (squares) [77].

In copper, a decrease in grain size and an increase in Vickers microhardness after HPT, ECAP, and accumulative roll bonding (ARB) correlate with an increase in electrical resistivity [127]. It is important to emphasize that various properties (grain size, hardness, torque, lattice parameter, resistivity, etc.) do not reach a steady state simultaneously.

2.2 Disordering and amorphization of alloys

The disordering of alloys under mechanical milling conditions was first discovered in Fe–Pt and Co–Pt systems [5], and

the phenomenon of amorphization in Y–Co [11] and Gd–Co [12] intermetallics. These studies stimulated interest in subsequent decades in unconventional phase transformations under SPD. Amorphization was also discovered shortly thereafter in mechanical alloying of a mixture of powders of pure Nb–Ni [15] and Ti–Ni [17] components. The results of further experimental studies are summarized in reviews [8, 9, 13, 14].

Despite the qualitative similarity between the final structural state upon amorphization of intermetallics (Y–Co, Gd–Co) and mechanical alloying of a mixture of powders (Nb–Ni, Ti–Ni), there is a striking difference in the forces that drive these transformations [9]. The formation of amorphous solid solutions in systems with negative enthalpy of mixing leads to a decrease in the free energy of the system, and this phenomenon can be explained in terms of equilibrium thermodynamics. However, the disordering and amorphization of intermetallics are accompanied by an increase in free energy, so under the effect of plastic deformation, the system moves away from thermodynamic equilibrium.

Possible driving forces responsible for the amorphization of intermetallics are listed in [137]: they are the difference between the enthalpies of the disordered and amorphous states and the stored energy of defects. A simple empirical criterion for the realization of an amorphous or disordered state in the presence of SPD was proposed in [8]: alloys with a large difference between the atomic radii of the components and the existence of intermetallics in the equilibrium phase diagram are prone to amorphization, while disordering without amorphization occurs in systems with close values of atomic radii (Fe–Pt, Co–Pt). It should be noted that the difference between the atomic radii of the components is also one of the conditions for amorphization under quenching from the liquid state [138, 139].

A thermodynamic explanation of the amorphization of intermetallics under SPD observed in many systems (CuZn, Nb_3Sn(Au), CoGa (Al), Co_2Ge(Si), etc.), has been proposed in [9]. The main driving force responsible for this process is an increment in enthalpy that results from the disordering of the alloy under SPD. If the enthalpy of the solid solution is less than that of the amorphous state (for example, in the Nb–Au system), only disordering of the intermetallic compound occurs under the effect of SPD and, as a result, a homogeneous solid solution is formed. Otherwise, the disordered state is unstable with respect to the transition to the amorphous phase.

A comparison of the enthalpies of a disordered solid solution and an amorphous state calculated using the semiempirical Miedema model [140] has shown that this explanation is adequate in 90% of cases. In another 5% of cases, the Miedema model gave a negative result, but the difference between the enthalpies of the amorphous state and the solid solution turned out to be insignificant, and it can be compensated by the unaccounted contribution of the energy of grain boundaries and other defects. On the whole, however, the contribution of the energy of accumulated defects was estimated in [140] as insignificant in comparison to that due to the disordering effect, and it rarely affects the final result. A disadvantage of this approach is that it ignores the entropic contribution to free energy. This contribution can be estimated using, instead of the Miedema model, the parameterization of free energy in the CALPHAD method (CALculation of PHAse Diagrams), which is based on the interpolation of experimental data. A comparison of these approaches carried out in [13] for Ni–Zr and Ti–Al systems has shown that the results obtained are sufficiently close, i.e., the contribution of entropy appears to be small.

The amorphous state is described in the microscopic approach either as a quasi-liquid (Bernal and Voronoi polyhedral models) [141] or as a pseudocrystal with a high density of defects (in particular, grain boundaries) [142]. The topological order in amorphous alloys is polytetrahedral, which is incompatible with the translational symmetry of crystals but can be achieved by introducing disclinations into the crystal [143]. Disclination-dislocation models of the amorphous state were considered in [144], and the concept of amorphization of alloys in the presence of SPD with the involvement of rotational modes was first formulated in [145].

At the same time, the kinetics of the transition to the amorphous state under SPD remains poorly understood. It was suggested in [146] that these kinetics are athermal, similar to those in the martensitic transition, which is responsible for the rapid realization of the transformation at low temperatures. However, the nature of the mechanism that ensures the cooperative nature of the transformation remains a matter of discussion. The accumulation of defects is apparently necessary for realizing the rearrangement of the atomic structure that ensures a change in the topological order (see the discussion in [147]). For example, it was experimentally shown in [148] that amorphization occurs in the Ti–Ni alloy at the shear band front.

The microscopic mechanism of alloy disordering, which precedes amorphization, is not entirely clear either. Typical kinetics of this process are shown in Fig. 3: at elevated temperatures of mechanical activation, the order parameter decreases with time and reaches a stationary value (which depends on the intensity of treatment), and at temperatures below the critical one, complete disordering occurs. A possible explanation of this phenomenon proposed in [14] refers to the atomic order breaking in the process of the slip of dislocations, the Burgers vector of which differs from the translation vector in the lattice of an ordered alloy. The passage of a single superparticle dislocation results in the emergence of an antiphase boundary (APB). The passage of many such dislocations in intersecting planes at sufficiently low temperatures (i.e., in the absence of processes that restore atomic order) leads to the formation of many intersecting APBs, extreme fragmentation, and disordering of the alloy.

To analyze this phenomenon, the authors of Refs [9, 14] employed the model of ballistic atomic jumps [149, 150], which is more adequate for alloys under irradiation. This model introduces, in addition to thermally activated diffusive jumps of atoms, additional jumps between the sublattices, which only depend on the intensity of the exposure. It follows from this assumption that, when the critical intensity of exposure is attained, the ordering completely vanishes. The ballistic model leads in the general case to the replacement of the actual temperature in the formula for the free energy with the effective one [149], which describes the upward shift of the point on the phase diagram that corresponds to the state of the alloy,

$$T_{\text{eff}} = T\left(1 + \frac{\Gamma_{\text{bal}}}{\Gamma_{\text{therm}}}\right), \tag{1}$$

where Γ_{bal} and Γ_{therm} are the frequencies of ballistic and thermally activated jumps.

The empirical conclusion regarding the effective shift of the figurative point of an alloy subjected to SPD to the high-

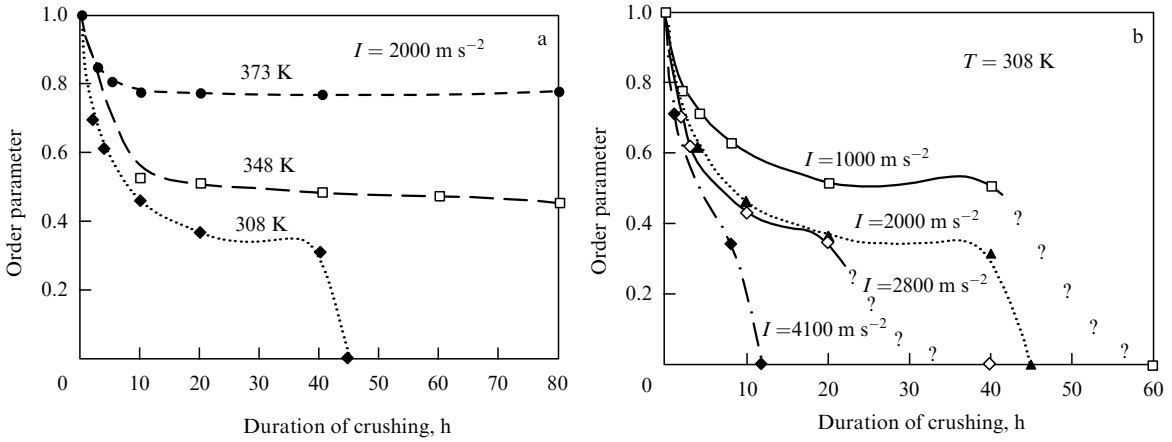

Figure 3. Typical evolution of the order parameter in the process of crushing by ball milling the $Fe_{50}Al_{50}$ intermetallic at various temperatures (a) and various intensities of processing (b) [153].

temperature region of the phase diagram is often valid not only for disordering, but also for the formation of supersaturated solid solutions and polymorphic transformations [62, 151, 152], which additionally stimulated interest in the Martin's ballistic model [149]. It was shown in [151] that the ballistic model is qualitatively valid for various transformations, including realization of amorphous phases (which are considered liquid phases in the equilibrium phase diagram).

Equation (1) shows that, if the SPD temperature is increased without changing the parameters of the deformation process, the frequency of thermally activated jumps Γ_{therm} increases; therefore, the effective temperature T_{eff} decreases. If the SPD temperature decreases, T_{eff} should increase. This phenomenon can be clearly seen in the HPT data for the alloys Ti–48.5 at.% Ni, Ti–50.0 at.% Ni, and Ti–50.7 at.% Ni [154]. The HPT of equiatomic alloy Ti–50.0 at.% Ni at room temperature (point e in Fig. 4) resulted in a completely amorphous state (point *5* in Fig. 4, $T_{\text{eff}} = 1350\,^{\circ}\text{C}$). The HPT of nonequiatomic alloy Ti–48.5 at.% Ni at $T = 270\,^{\circ}\text{C}$ (point h) resulted in the formation of a mixture of amorphous and nanocrystalline phases (point *7*, $T_{\text{eff}} = 1050\,^{\circ}\text{C}$). If the HPT temperature of the Ti–48.5 at.% Ni alloy increases to $T_{\text{eff}} = 1050\,^{\circ}\text{C}$ (point i), a mixture of nanocrystalline phases alone without an amorphous phase is formed. This implies that the corresponding point moved from position *7* in the region $\delta + \text{L}$ to position *8* in the two-phase region $\delta + \gamma$, and the effective temperature decreased to $T_{\text{eff}} = 950\,^{\circ}\text{C}$. The HPT of another nonequiatomic alloy Ti–50.7 at.% Ni at $T = 200\,^{\circ}\text{C}$ (point j) yields a mixture of amorphous and nanocrystalline phases (point *9*, $T_{\text{eff}} = 1250\,^{\circ}\text{C}$). If the HPT temperature of the alloy Ti–50.7 at.% Ni increases to 250 °C (point k), a mixture of nanocrystalline phases alone without an amorphous phase is formed. This implies that the corresponding point moved from position *9* in the region $\delta + \text{L}$ to position *10* in the two-phase region $\delta + \beta$ and the effective temperature decreased to $T_{\text{eff}} = 1100\,^{\circ}\text{C}$. Therefore, the data obtained in [154] clearly show that an increase in the temperature of HPT treatment results in a decrease of T_{eff}, which fully corresponds to Eqn (1).

It should be noted that the conditions for the applicability of model [14, 149] are very stringent (homogeneity and high intensity of plastic deformation, weak manifestation of relaxation processes), which, in our opinion, does not fully

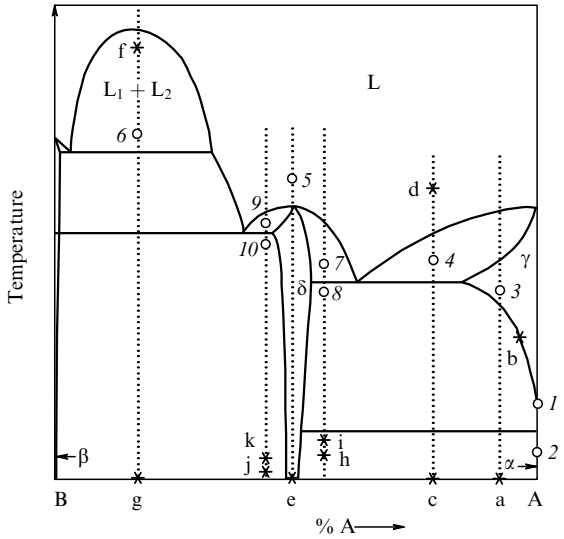

Figure 4. Schematic binary phase diagram. Corresponding figurative points at (elevated) effective temperatures T_{eff} are shown by numbered circles. Dotted vertical lines represent the compositions of the various alloys. Each asterisk with a letter indicates the composition and temperature of processing of the alloy (normal cooling, SPD, or rapid cooling) (see details in the text).

agree with the experimental situation. Disordering has been observed in some studies (see [6]) even at a low intensity of treatment by rolling or drawing.

The disordering of an alloy during SPD was considered in [155] in a model that assumes a decrease in the ordering temperature in the region of structural defects (dislocations, grain boundaries); disordering occurs in this case at moderate temperatures locally, through diffusion over short distances (of the order of the lattice parameter) in the region of the defect, and the attained nonequilibrium state is frozen after the displacement of the defect due to the low rate of bulk diffusion $D_{\text{GB}}/D_{\text{bulk}} \gg 1$ (Fig. 5a). As a result, similar to the diffusionless mixing model [14], an effective shift of the figurative point of the compound to the high-temperature region of the phase diagram may be discussed. Disordering is realized most efficiently at a certain optimal velocity v of motion of the defect (Fig. 5b); at smaller values of v, the atomic order is restored behind

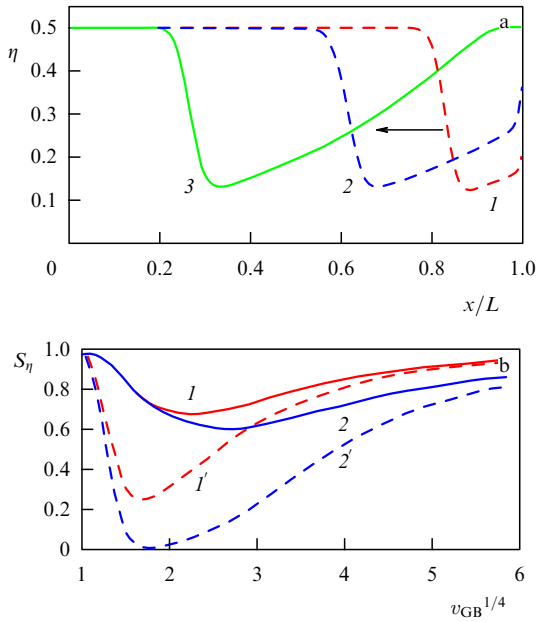

Figure 5. (a) Profiles of the order parameter η at various moments of time when the defect moves from the position $x/L = 1$, $D_{GB}/D_{bulk} = 10^2$. (b) Degree of ordering averaged over the sample $S_\eta = 2L^{-1}\int|\eta(\mathbf{r})|d\mathbf{r}$ as a function of the velocity of motion of the defect v_{GB} after the first pass (*1*, *1′*) and after five passes (*2*, *2′*); $D_{GB}/D_{bulk} = 10^2$ (curves *1*, *2*), 10^5 (curves *1′*, *2′*) [155].

the defect, while at large v, the disordering does not have enough time to occur. Therefore, the degree of ordering may significantly decrease during dynamic recrystallization, when active migration of grain boundaries occurs. However, a high density of defects is not necessarily attained in this situation.

At the same time, it was suggested in [62, 156] that the main cause of nonequilibrium transformations under SPD (including amorphization) is the accumulation of a large number of structural defects in the bulk of the material. In the opinion of the authors of [62], it is the accumulated energy of defects that provides an effective shift of the figurative point of the alloy to higher temperatures in the phase diagram. Amorphization occurs if the effective temperature is in the phase diagram region that corresponds to the liquid phase. For example, amorphization during SPD in the $Nd_2Fe_{14}B$ system is combined in this case with decomposition, i.e., is probably realized under conditions of rapid diffusion, which, however, fails to ensure the restoration of the ordered phase [50, 157, 158]. It should be emphasized that for a significant effect to be attainable in the approach of Ref. [62], it is necessary to accumulate many defects in the bulk of the material, a requirement that does not have clear experimental evidence.

According to [62, 159], vacancies may play a significant role in increasing the free energy of the alloy and its transition to the amorphous state. However, it is difficult to agree with this assertion, since the presence of a large number of vacancies uniformly distributed over the sample should result, primarily, in the acceleration of bulk diffusion and, consequently, in the restoration of the thermodynamic equilibrium state.

The authors of Ref. [160] emphasized, in particular, the possible significant role of nonequilibrium vacancy flows in the amorphization of alloys under SPD. If there are sources and sinks of vacancies at the grain boundaries and junctions that are effective for a long time, the alloy stratifies according to the mechanism of the inverse Kirkendall effect [161, 162] due to the difference in diffusion mobility among atoms of different types. Amorphization occurs if the free energy of the inhomogeneous alloy is greater than that of the amorphous state. If, in addition, it is assumed that the spatial configuration of the sources and sinks of vacancies varies slowly, the attained stratification of the alloy can eventually be replaced by homogenization, which, according to [160], explains the cyclic amorphization-crystallization reaction in the $Co_{75}Ti_{25}$ alloy [53].

The approach formulated in [160] involves a number of assumptions that can hardly be argued for. In particular, there are no experimental facts that would indicate the stratification of alloys into layers of various compositions in the process of amorphization. Moreover, calorimetric studies have been performed in the $Co_{75}Ti_{25}$ alloy [53] (in which a cyclic amorphization-crystallization reaction during treatment has been observed) and a number of other systems [9], in which the amorphous phase only featured a single narrow peak, which apparently indicates the homogeneity of the amorphous state.

It is known that amorphization in irradiated crystalline thin films is explained by the generation and accumulation of defects (vacancies and interstitial atoms) in the course of treatment [163, 164]. The crystal→amorphous state phase transition occurs in this case if the free energy density of the crystalline phase with defects becomes equal to that of the amorphous phase. Attempts to extend these concepts to amorphization of alloys in the presence of SPD have been made for a long time [156, 165]. However, the energies of various states estimated in the Miedema model presented in review [9] show that the main reason for the amorphization of the alloy under SPD is the transition to a disordered state, which, in turn, is more likely due to more effective kinetic factors accompanying SPD rather than to a change in the thermodynamic properties of the alloy due to the accumulation of defects. This conclusion is indirectly confirmed by the observation that examples of amorphization of pure metals or equilibrium disordered alloys under SPD are virtually unknown.

2.3 Formation of supersaturated solid solutions and highly dispersed states

2.3.1 Experimental results. SPD is a promising method for alloying steels and alloys, especially in those cases when it is not possible to obtain a supersaturated solid solution (SSS) using an alternative technique [166-168]. In substitutional alloys with low mutual solubility of components, such as Fe–Cu [169–175], Fe–Pb [176], Fe–Sn [177], Fe–Mg [178,179], Cu–Ag [180–182], Cu–Co [183–185], Cu–Cr [186], Cr–Mo [187], Cu–Ta [188], and Zr–Nb [152], solid solutions are supersaturated by several tens of percent during processing at low ($T < 300$ K) or moderate temperatures. The final product may be a homogeneous crystalline phase, a heterogeneous state, or an X-ray-amorphous solid solution. At the same time, the SSS could not be obtained in the Fe–Ag system even at $T = 77$ K [189]; in Ni–Ag [190] and Cu–Mo [191], only partial homogenization was observed, while in the Cu–Co [151], Al–Zn, and Al–Mg [81] systems at $T \approx 300$ K, the SSS obtained by quenching from high temperatures experienced anomalously fast decomposition.

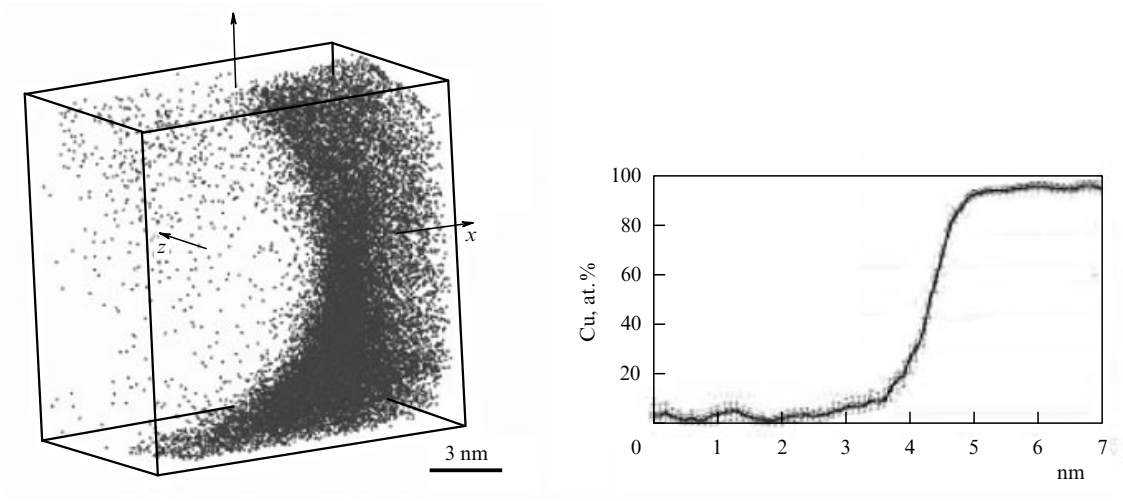

Figure 6. Distribution of Cu atoms near the interface between phases that is formed in the process of mechanical alloying in the Fe–Cu system at $T = 300$ K [173].

The characteristic features of the kinetics of SSS formation include the emergence of anomalously wide interphase boundaries [170, 173] (Fig. 6) and the independence of the magnitude of the effect on temperature at $T < 300$ K [174]; at low temperatures, the degree of dissolution of precipitates is proportional to the actual deformation, which is determined by the number of dislocations that pass through the grain [32, 174].

Of particular interest is the dissolution of precipitates of various phases in the process of SPD. The dissolution of carbides during cold deformation of steel has been studied in detail in [36]. A sequence of transformations has been observed in high-carbon steel U13 under the effect of SPD:

$$\alpha\mathrm{Fe} + \mathrm{Fe_3C} \rightarrow \alpha\mathrm{Fe} - \mathrm{C} \rightarrow \varepsilon + \chi + \gamma\mathrm{Fe} - \mathrm{C} \qquad (2)$$

(when cementite dissolves, solid α- and γ-solutions are formed from which secondary carbides ε, χ precipitate) [192]. References [37, 112, 193, 194] explored the dissolution of cementite in steel under SPD. The dissolution of nitrides [38] and oxides [33–35] in the αFe matrix and other metals was also investigated. Mechanically induced dissolution of CrN nitride in the αFe–Ni alloy matrix was used in [39] to obtain γFe–Cr–Ni–N austenitic stainless steel.

Structural features were observed in SPD of alloys at moderate temperatures $T \sim 450$ K, which are a consequence of the competition between the processes that move the alloy away from thermodynamic equilibrium and normal diffusion, which returns the system to the equilibrium state. For example, dispersed structures in the form of lamellae were observed in the Ag–Cu system [29, 30], which retain their morphological features under intense exposure, a feature which is a characteristic signature of self-organization (Fig. 7). The lamella width increased from 1 to 10 nm if temperature increased from 393 K to 453 K, while at lower temperatures a homogeneous state was formed. The competition between the processes of mechanical alloying and the decomposition of the solid solution also occurs, apparently, in the Cu–Co [185] and Fe–Cr [40] systems, where highly dispersed states with signs of composition modulation were obtained in the process of SPD. For example, the same dispersed state was obtained in the Fe–Cr system with a characteristic scale of concentration inhomogeneity of several

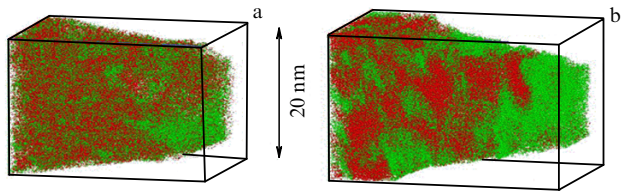

Figure 7. (a) Mechanical alloying of Ag–Cu alloy powder in a ball mill at $T = 393$ K. (b) Concentration inhomogeneity areas formed at a deformation temperature $T = 453$ K [30].

nanometers from the initial state, which is homogeneous or consists of a mixture of pure component powders.

As discussed above, the grain size decreases or increases under SPD, depending on whether it is larger or smaller than the stationary value (see Fig. 2). This is also true for SPD-induced hardening/softening. A similar situation also occurs in the case of dissolution/precipitation. A certain concentration c_{ss} is attained in the steady state in a solid solution, the value of which is controlled by the dynamic equilibrium between dissolution and precipitation. If the initial concentration c_{init} of the solid solution is lower than c_{ss}, it increases under SPD, and the particles of the second phase dissolve. If $c_{init} > c_{ss}$, the concentration of the second component in the solid solution decreases, and new precipitates emerge (so-called dynamic aging). This aging, which was first observed in Al–Zn alloys [135], is now actively used to control the properties of materials [195].

The competition between the dissolution of particles and the decomposition of a supersaturated solid solution has been studied in detail in binary copper alloys [28]. The steady-state concentration c_{ss} is established in the solid solution due to the effect of these processes during SPD. To compare binary alloys having different maximum solubility values of the second component, it is useful to introduce the so-called effective temperature T_{eff} (see Eqn (1)): the concentration c_{ss} of the second component in the matrix after SPD is such, as if the sample was annealed until equilibrium corresponding to a certain (elevated) temperature T_{eff}.

We now consider an example of the competition between dissolution and decomposition in the Cu–Co system [98, 196, 197]. The Cu–4.9 wt.% Co alloy contained grains of a copper-based solid solution 10–20 μm in size, cobalt particles about

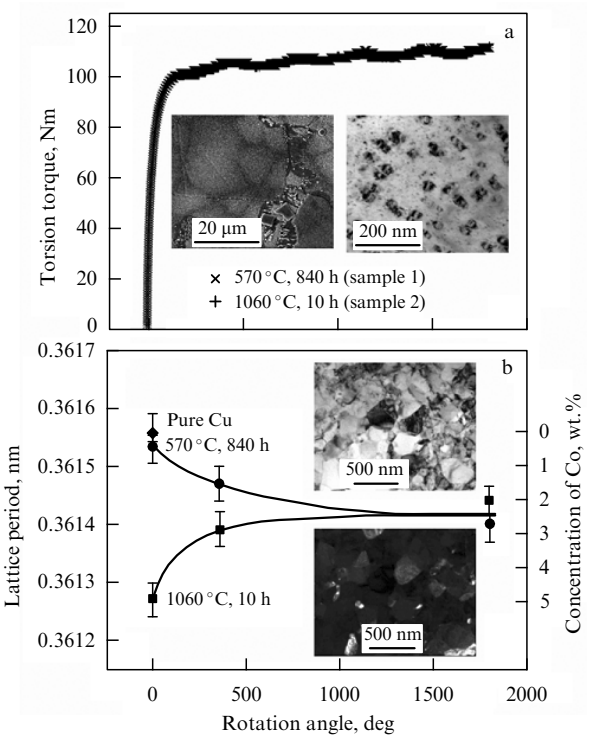

Figure 8. (a) Torque as a function of the rotation angle. The insets show micrographs of the Cu–4.9 wt.% Co alloy after annealing at $T = 570\,^{\circ}\mathrm{C}$ for 840 h obtained by scanning electron microscopy (left) and bright-field transmission electron microscopy (TEM) (right). (b) Lattice period as a function of the anvil rotation angle. The dots mark the lattice parameter in sample 1 annealed at $T = 570\,^{\circ}\mathrm{C}$ for 840 h. The squares correspond to sample 2 annealed at $T = 1060\,^{\circ}\mathrm{C}$ for 10 h. The diamond marks the lattice period for pure copper. The corresponding concentration of cobalt is shown on the right vertical axis, $c_{eq} \approx 2.5$ wt.% Co. The insets show bright-field (top) and dark-field (bottom) TEM micrographs of the Cu–4.9 wt.% Co alloy after annealing at $T = 570\,^{\circ}\mathrm{C}$ for 840 h and HPT (6 GPa, 5 revolutions, 1 revolution per minute) [98].

2 μm in size, and finely dispersed cobalt precipitates formed during HPT with a particle size of ≈ 10–20 nm [98, 196, 197]. Cobalt completely dissolved in the copper matrix after annealing at $T = 1060\,^{\circ}\mathrm{C}$ for 10 h. The grain size after this annealing was ≈ 50 μm. The copper-based solid solution almost completely decomposed in the process of annealing at $T = 570\,^{\circ}\mathrm{C}$ for 840 h: less than 0.5 wt% Co remained dissolved in the copper (as the data of X-ray structural measurements and the phase diagram show [98]).

After HPT of both samples, the copper grain size sharply decreased to about 200 nm, and the cobalt particle size, to 10–20 nm (see insets in Fig. 8b). The torque in both samples attained a stationary value after a short growth period during the first revolution of the anvils (Fig. 8a). Figure 8b shows the lattice parameter in sample 1 annealed at $T = 570\,^{\circ}\mathrm{C}$ for 840 h (dots) and sample 2 annealed at $T = 1060\,^{\circ}\mathrm{C}$ for 10 h (squares) as a function of the rotation angle. The lattice parameter of sample 1 before deformation is very close to that of pure copper (the diamond in Fig. 8b). As the number of revolutions increased, the lattice parameter of sample 1 decreased, and that of sample 2 increased. The lattice parameters in both samples after five revolutions of the anvil were virtually indistinguishable and corresponded to a solid solution of cobalt in copper with ≈ 2.5 wt.% Co. In other words, the composition of the solid solution in the Cu–4.9 wt.% Co alloy after HPT does not depend on the initial pre-HPT state. This is the so-called equifinal composition: $c_{eq} \approx 2.5$ wt.% Co.

Thus, the steady state with respect to grain size, cobalt precipitate size, and cobalt concentration in a solid solution under HPT is indeed equifinal. The Cu–Co phase diagram shows that the solid solution in samples 1 and 2 after HPT contains the same amount of cobalt, $c_{eq} \approx 2.5$ wt.% Co, as if these samples were annealed at $T_{eff1} = 920 \pm 30\,^{\circ}\mathrm{C}$ and $T_{eff2} = 870 \pm 30\,^{\circ}\mathrm{C}$, respectively.

An analogy arises here between thermodynamic equilibrium, where the composition of the phases does not depend on the initial state, and the situation where the composition of the phases in the stationary state during SPD is also independent of the initial-state phases. The characteristics such as the equivalent (effective) temperature T_{eff} and the stationary (equifinal) composition of solid solutions c_{eq} are often referred to as attractors in the thermodynamics of open systems [198].

The values of T_{eff} for several Cu-based alloys were compared in [28]: Cu–Ni [43], Cu–Co [98, 196, 197], Cu–Sn [199–201], Cu–In [202, 203], Cu–Cr [204], Cu–Ag [205–207], Cu–Al–Ni [208, 209], and Cu–Hf [28]. The value of T_{eff} increases linearly with an increase in the activation enthalpy of bulk diffusion. A correlation has also been found between the activation enthalpy of bulk diffusion and the melting point of the diffusing alloying component T_m. As a result, T_{eff} increases linearly with increasing temperature T_m of the alloying component. The observed correlations enable a prediction of phase transitions in copper alloys under HPT. Thus, the temperature T_{eff} is a parameter convenient for discussing the qualitative features of phase transformations under SPD. However, a method for calculating this quantity has not yet been proposed, and the microscopic mechanisms that determine its change have not been specified.

2.3.2 Model concepts. To explain the formation of a supersaturated solid solution, the following models have been proposed: a model of local heating in contact with grinding bodies in ball mills [210]; a model of dissolution of equilibrium phases due to the accumulated energy of defects [62], in particular, the high energy of grain boundaries [188]; a model that interprets SSS as a metastable state thermodynamically caused by the accumulation of interstitial atoms in the bulk of the material [68, 211, 212]; a model of direct mechanical mixing due to dislocation slip with completely frozen diffusion [58, 213]; a model of diffusive dissolution of subcritical precipitates emerging under SPD [26, 173, 184]; a model of the growth of nonequilibrium phases due to the relaxation of amorphous boundaries between powder particles (in a mixture of pure components) [171, 186]; and a model of 'diffusive cutting' and dissolution of precipitates by dislocations and dislocation clusters as a result of a local change in the chemical potential in the region of defects [60, 61, 214]. There is currently no unified point of view on the physical nature of the observed phenomenon. We discuss below some of the approaches listed above.

Abnormal mechanical alloying (in systems whose decomposition is thermodynamically stimulated) develops more actively if the processing temperature in ball mills is decreased and the size of the balls is diminished, i.e., when local heating is suppressed [186]. This phenomenon is observed not only in ball mills, but also in other processing methods, for example, in torsion under high pressure, when local heating is excluded [174]. Thus, the local heating model

[210] draws attention to possible artifacts in the case of alloy processing in ball mills, rather than explaining the physical essence of the phenomenon.

The concept of dissolution of phase fragments of subcritical size [26] that emerge in the process of mechanical cutting of precipitates by dislocations originates from the general principles of thermodynamics. However, it is necessary to take into account the competing growth of large precipitates and the nucleation of new precipitates in a solid solution. The critical size of the nucleus tends to infinity at the boundary of two-phase region of the phase diagram, but rapidly decreases upon cooling [215]. For example, according to experiments [216], this size is only ≈ 0.2 nm in the $Fe_{0.99}Cu_{0.01}$ solid solution with a body-centered cubic (bcc) lattice at $T = 770$ K, and at lower T, any cluster consisting of several atoms is capable of growth. Therefore, the area of applicability of this concept is limited to a situation in which the phase diagram point of the solution is located near the boundary of two-phase region of the phase diagram, and bulk diffusion is quite intense.

The concept of the decisive role of the stored energy of defects [62] (for example, grain boundaries [188]) in dissolution of phases under SPD partly reflects the observed trends, but says nothing about the kinetic mechanism that ensures homogenization of the alloy. Moreover, the stored energy of the alloy, due to the high density of grain boundaries (GBs) after SPD, can lead to the opposite outcome due to the formation of segregations and grain boundary decomposition. The role of the accumulated energy of defects is reduced in [62] to the effective shift to the high-temperature region of the phase diagram. However, the relationship between the displacement of the figurative point and the accumulated energy is not obvious, while effective heating emerges in model approaches as a kinetic effect due to direct mechanical mixing [9, 58, 149]. The most substantiated study is apparently [68], in which the formation of supersaturated solid solutions under SPD is explained by a change in thermodynamic properties as a result of the accumulation of about 1 at.% of interstitial atoms (the concentration of defects is estimated using the change in the average lattice parameter after SPD). However, the obtained estimate of the stored energy of interstitial defects (3.5 kJ mol^{-1}) turns out to be an order of magnitude less than the typical value of the mixing energy.

Direct mechanical mixing [14, 58, 213] in shear bands may explain mechanical alloying observed at extremely low temperatures, ~ 80 K. The mechanism of this phenomenon is illustrated by the results obtained by Monte Carlo computer simulations [14] and molecular dynamics [213, 217] techniques. Direct mixing is introduced in theoretical models [149] by postulating ballistic jumps of atoms in addition to normal diffusion, which leads to an effective upward shift in temperature in the phase diagram, in agreement with the results of [62, 151, 152]. The direct mixing mechanism is clearly supported by the observation that the degree of homogenization of the Fe–Cu alloy during processing at low temperatures ranging from 77 K to 300 K weakly depends on the exposure rate (and temperature), but is only determined by the magnitude of plastic deformation [174]. The simulation of shear deformation at moderate temperatures revealed a competition between direct mixing and diffusion-controlled decomposition that results in the formation of dissipative structures (patterns) [58], in agreement with experimental observations for the Ag–Cu system [30].

Although the concept of mechanical mixing is now quite popular, many authors note that the required uniform plastic deformation is virtually unattainable [32, 218]. Moreover, the formation of a supersaturated solid solution is only observed in a number of systems (Fe–Pb [176], Fe–Sn [177]) after transition to the nanocrystalline state, when the slip of dislocations in the bulk of grains is suppressed [64, 219, 220]. Transmission electron microscopy of the Fe–Cu alloy after HPT revealed no signs of crossing the boundaries of precipitates by dislocations, which is also an indirect indication of the absence of direct mechanical mixing [174]. It is possible that it occurs in nanocrystalline materials not in the bulk, but at the boundaries of grains with high migration mobility (in particular, dynamic recrystallization is observed at room temperature [221–223] and possibly even at cryogenic [174] temperatures).

It is of importance to note that, at least at moderate temperatures (in particular, close to room temperature), diffusion apparently is also involved in mechanical alloying. An argument in favor of this assertion is the experimental observation that solid solutions and intermetallics first emerge in the process of SPD on the side of the low-mobile component [68, 224, 225], which cannot be ensured by direct mixing. Moreover, based on the concept of direct mixing, it is impossible to understand why the dissolution of copper precipitates in an iron matrix occurs in two stages: first, the precipitates of face-centered cubic (fcc) copper are saturated with iron up to 11 at.%, and only after that a supersaturated solid solution of copper in αFe is formed [170, 171].

2.3.3 Diffusive cutting and dissolution of precipitates by dislocations and grain boundaries. To explain the dissolution of fine precipitates of equilibrium phases in the process of SPD at moderate temperatures, models have been proposed based on the concept of the development of diffusion processes in the dislocation region [60, 61, 155, 214] and grain boundaries [155, 226, 227] with the possible 'freezing' of the attained state after the displacement of defects.

Studies [60, 61] explored a situation in which the applied stress is insufficient for mechanical cutting, so the ensemble of dislocations stops at the precipitate boundary. Further evolution is due to the elastic interaction between the atoms that form the precipitate with the edge components of the dislocations. Flows of atoms emerge as a result between the regions of compression and tension of the lattice near the dislocation, and the shape of the precipitate changes with time; the ensemble of dislocations (under the effect of the applied stress) moves into the region previously occupied by precipitates. In essence, this model describes not dissolution, but rather the so-called diffusive cutting of precipitates, the rate of which is limited by diffusion. Experimental observations indicate (see, for example, [32]) that precipitates that dissolve under SPD have both large and small lattice parameters (in comparison with those of the matrix), contrary to the conclusions in [60, 61], according to which only those precipitates whose lattice parameter is greater than that of the matrix dissolve. There is at present no doubt that the elastic contribution is far from the only contribution that determines the interaction between dissolved atoms and other lattice defects [228].

A more general approach to the dissolution of precipitates in the process of their interaction with dislocations was discussed in [214, 227]. It was taken into account that the thermodynamic properties of the alloy (the energies of

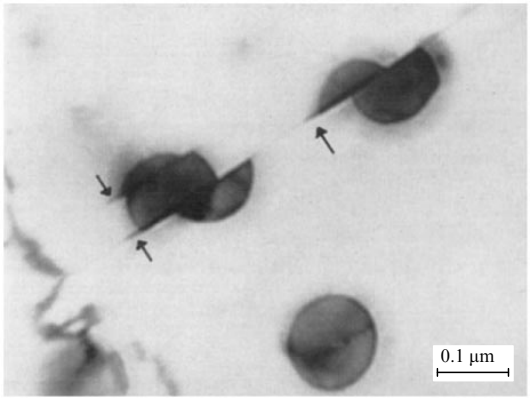

Figure 9. Cutting of Ni_3Al particles by dislocations in the process of cold deformation of an aged 75Ni–19Cr–6Al (at.%) alloy [218].

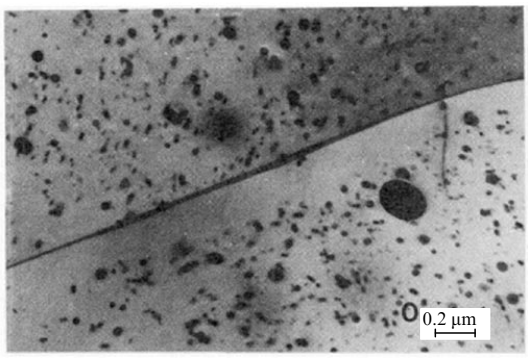

Figure 10. Dissolution of precipitates in the Ti–Y–O alloy in the wake of a moving grain boundary [218].

segregation, mixing, and ordering) change near the dislocations that cut the precipitates, which facilitates local development of the transformation. When a dislocation is displaced, the state that is formed is frozen until the next dislocation arrives, so the alloy moves away from the state of thermodynamic equilibrium in the process of deformation. It should be noted that studies [214, 227] did not explore (similar to [60, 61]) effects associated with rapid diffusion along dislocation tubes, which may prove to be decisive at moderate temperatures. In discussing the dissolution of interstitial phases, it is also necessary to take into account the possibility of capturing of Cottrell impurity atmospheres [229] by moving dislocations [32], since interstitial atoms usually have high diffusion mobility and a significant energy of binding with dislocations.

The dissolution of precipitates upon contact with dislocations has been reliably confirmed in experiments. The dissolution of the Guinier–Preston zones and the metastable θ'-phase in the cold plastic deformation of the Al–Cu alloy was discovered in [230]. It was observed in [218] that a group of dislocations cut the γ'-particle Ni_3Al in the 75Ni–19Cr–6Al alloy (at.%); it was shown that the dislocations not only mechanically cut the particle, but also carry nickel atoms out of its limits, a phenomenon that manifests itself in the form of long 'tails' of impurity atoms (Fig. 9). Diffusive cutting and dissolution of intermetallic particles in the Fe–Ni–Ti austenitic alloy were observed in [231]. Reference [232] showed for the first time that carbides may dissolve as a result of being intersected by dislocations. Three-dimensional (3D) atomic tomography [233–236] indicates the scale of impurity atmospheres at dislocations: for example, the Mn concentration in dislocation tubes increases in the substitutional bcc-$Fe_{91}Mn_9$ alloy to 30% [236].

Recent studies [237, 238] have shown that particles of the Ni_3Ti and Ni_3Al phases in austenitic steel, for which the dissolution mechanism is known to be diffusive cutting, dissolve more efficiently at low temperatures, down to 77 K. It is hypothesized that the diffusive cutting by dislocations is realized in this case not by a vacancy, but by a crowdion diffusion mechanism, which has a lower activation energy, and therefore is advantageous at low T. The effect of this mechanism may be extended to many systems for which direct mixing was previously considered to be the only possible mechanism of transformation under SPD.

The effect of dissolution of precipitates by moving grain boundaries, first discovered in [239], is observed experimentally at elevated temperatures, when recrystallization and diffusion phase transformations may occur concurrently. It was found in [155, 240, 241] that nanosized precipitates of Al_3Zr and yttrium in the Al–Cr–Zr and Ti–Y–O systems decrease in size or dissolve in the wake of moving grain boundaries (Fig. 10). The dissolution of precipitates in Cu–Co, Ni–Al, Al–Cu alloys in the process of recrystallization was noted in [242]. The dissolution of coherent $Y_xTi_yO_z$ precipitates in oxide dispersion-strengthened ferritic steel due to the migration of GBs has been observed recently [243]. These observations show the conceptual possibility of the dissolution of precipitates by moving GBs. Similar processes may develop in the case of SPD, which is usually carried out at lower temperatures, in the process of low-temperature dynamic recrystallization [65].

Grain boundaries play an important role in mechanical alloying in many systems. For example, in the $Fe_{95}Pb_5$ alloy (with the ratio of atomic radii $R_{Pb}/R_{Fe} = 1.41$ and the absence of solubility under equilibrium conditions), first, Pb atoms segregate during exposure at the boundaries of αFe grains, and only at the next stage, during the transition to the nanocrystalline state, is a supersaturated solid solution formed [176]. The dissolution of the phases occurred in the $Fe_{68}Sn_{32}$ system when the grain size was 3–5 nm [177], while in the $Fe_{93}Mg_7$ system, it occurred when the grain size decreased to 10 nm [179]. Although GBs determined the process kinetics in all cases, impurity atoms of lead, magnesium, and tin were distributed in the final state uniformly over the entire volume of αFe grains. Thus, the role of GBs was not limited to the formation of segregations. However, the hypothesized important role of GBs in the formation of a SSS has been questioned for the Fe–Cu system [244], since the change in the enthalpy at GBs in this system is small compared to the contribution from the mixing energy.

A model for the dissolution of fine precipitates was proposed in [245], which is based on the calculated profile [246, 247] of the impurity concentration near a moving GB. According to [245], fine precipitates dissolve in the depletion zone near the GB provided that their size is comparable to the width of this zone, and the boundary velocity is not too high. This model considers in essence one of the possible mechanisms of local change in the thermodynamic conditions in the alloy near the GB; however, similarly to model [60, 61], it does not take into account the possibility that the GB passes through the precipitate.

A more general model that describes the passage of defects (GBs or dislocations) through precipitates and at the same

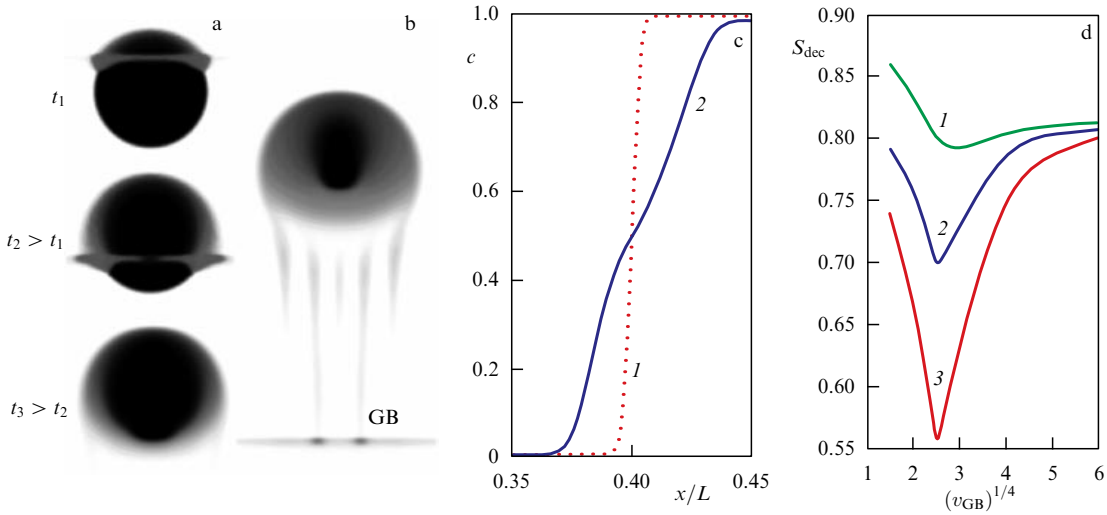

Figure 11. Distribution of the component concentration at various moments of time (a) upon single passage of the defect through the precipitate, $D_{GB}/D_{bulk} = 10^5$ [155], and (b) after five passages. (c) Profiles of the component concentration at the interface of the initial precipitate (curve *1*) and after passage of the defect (curve *1*). (d) Degree of decomposition as a function of the velocity of defect motion after one (curve *1*), five (curve *2*), and fifteen (curve *3*) passages of the defect.

time takes into account both the change in the energy of alloy components and the acceleration of diffusion in the region of extended defects was proposed in [155]. When a defect passes through a precipitate, the difference in the segregation energy on the defect in different phases leads to the emergence of flows of alloying element atoms outward from the precipitate volume. Partial dissolution of the precipitate and anomalous broadening of the interface occur as a result (Fig. 11a–c). While the magnitude of the effect is determined in the case of immobile defects by their segregation capacity (which is usually small compared to that of the bulk of the material), it is determined in the case of moving defects by the volume swept during motion. After the defect is displaced, the attained nonequilibrium state of the alloy is frozen due to the difference between the coefficients of bulk diffusion and diffusion along grain boundaries or dislocations ($D_{GB}/D_{bulk} \gg 11$). Figure 11d shows that, if the number of passes is fixed, there is an optimal velocity v at which the precipitates dissolve most efficiently; at low velocities v, segregations are entrained by the defect, while at high velocities, the transformation does not have enough time to develop in the defect region (however, it resumes when the next defect passes).

If the external action persists for a long time and the temperature is high (when not only diffusion at the defect but also the competing bulk diffusion are in effect), stationary dispersed states (dissipative structures) can be realized [155] (Fig. 12). A quasiperiodic distribution of concentrations is formed, i.e., a kind of reversal of spinodal decomposition occurs.

Thus, the two main mechanisms of formation of supersaturated solid solutions under SPD should be distinguished. The first, which is supported by computer simulations [14, 58], dominates at low temperatures (~ 77 K) and is reduced to direct mechanical 'mixing' of atoms as a result of the passage of intense dislocation flows localized in shear bands or during GB displacement. The implementation of mechanical alloying at low temperatures in nanocrystalline alloys, where dislocation slip in the bulk of grains is suppressed, suggests active GB migration in the course of exposure. The

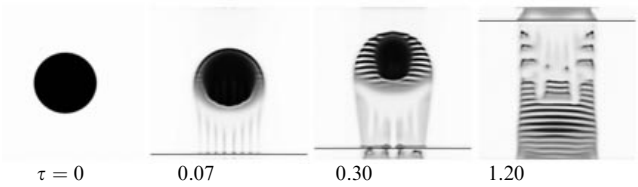

Figure 12. Kinetics of the formation of a disperse state (dissipative structure) as a result of multiple passage of a defect through a precipitate in a problem with periodic boundary conditions, $D_{GB}/D_{bulk} = 100$ [155].

second mechanism, which plays an important role at moderate temperatures (300–700 K), is due to a local change in the thermodynamic characteristics of the alloy and the acceleration of diffusion in the region of dislocation cores and moving GBs. It is supported by direct observations of local dissolution of precipitates in locations of dislocation clusters or behind a moving grain boundary.

2.4 Abnormal decomposition of alloys and compounds, cyclic reactions

As shown in Refs [50, 157, 158], shear under a pressure of 5–11 GPa in Bridgman anvils results in the decomposition of the equilibrium tetragonal $Nd_2Fe_{14}B$ phase into an amorphous phase enriched in neodymium and αFe nanocrystals. Low-temperature annealing ($T = 200-500\,^{\circ}C$) stimulated additional decomposition, while high-temperature annealing ($T > 500\,^{\circ}C$) restored the equilibrium phase composition. It has been noted previously [248–250] that the amount of αFe in *R*–Fe–B systems (where *R* is a rare-earth element) increases during prolonged grinding in ball mills; this, however, was explained for a long time by the contamination of the powders in the process of grinding. The decomposition of the Fe_2B compound during SPD was studied in [52] to show that it proceeds in two stages. First, the intermetallic is disordered and partially amorphized, then its separation occurs: $Fe_2B \rightarrow dFe_2B \rightarrow \alpha Fe + B$ (dFe_2B is a disordered phase); thus, abnormal decomposition occurs under altered thermodynamic conditions. A

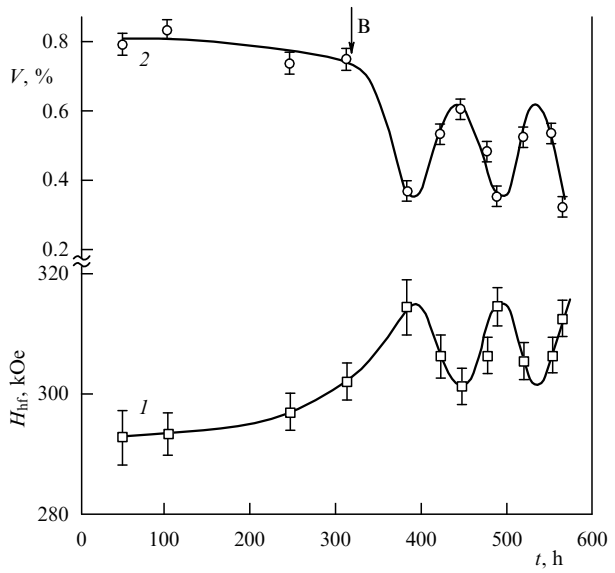

Figure 13. Average hyperfine field H_{hf}-(curve *1*) and the volume of the boron-containing phase (curve *2*) as functions of the time of mechanical processing in a mill of Fe + 50 at.% B mixture [54].

complex chain of transformations,

$$\beta\mathrm{FeB} \rightarrow \alpha\mathrm{FeB} \rightarrow \beta\mathrm{FeB} + \alpha\mathrm{FeB} \rightarrow \beta\mathrm{FeB} + \mathrm{Fe_2B} + \text{amorphous phase} + \mathrm{B} \rightarrow \alpha\mathrm{FeB} + (\mathrm{Fe_2B}) + \text{amorphous phase} + \mathrm{B},$$

with possible cyclicity of phase transformations was observed in [251]. It was shown in [54] that in processing a mixture of iron and boron powders in a ball mill, the proportion of the boron-containing phase can periodically vary with time (Fig. 13).

According to common concepts [9, 62], the amorphous phase may be considered a supercooled liquid phase, and its emergence corresponds to a shift of the phase-diagram point corresponding to the state of the alloy to the high-temperature region of the phase diagram. For example, the decomposition of the equilibrium phase $Nd_2Fe_{14}B \rightarrow$ amorphous phase + αFe is explained in [62] as follows. The corresponding diagram of states contains a high temperature region liquid + iron (delta and gamma). The alloy stores energy in the process of deformation and in a sence 'heats up' to the temperature of this region, as a result of which the observed transformation occurs. The external exposure results in this case in the realization of the amorphous phase and the acceleration of diffusion, while the abnormal decomposition is explained by the effect of thermodynamic stimuli under the changed conditions.

An alternative approach [155] is that equilibrium with the matrix phase may not be attained at sufficiently low temperatures due to the absence of bulk diffusion. Instead, a nonequilibrium transformation takes place under locally changed thermodynamic conditions, in shear bands. Indeed, the amorphous phase not returning to the crystalline state in the Nd–Fe–B system may be an indication of suppressed bulk diffusion. The formation of αFe nanocrystals under SPD in amorphous iron alloys usually occurs in this case in shear bands [252].

An example with cyclic reactions in the Fe–B system [54] shows that the concept of the displacement of the figurative point of the alloy in the equilibrium phase diagram is not always comprehensive. To explain the observed phenomenon, the authors employ concepts of nonequilibrium thermodynamics [253, 254], which adopts as the steady state behavior of the system not only equilibrium states of matter, but also dynamic stationary regimes. If local boron concentration $C_B < 16$ at.%, a bcc structure with a coordination number $z = 8$ is preferable, while if iron is saturated with boron up to $C_B = 25$ at.%, the fcc structure becomes preferable, in which $z = 12$. The actual structure that emerges in the process of exposure is a mixture of the two indicated states. The saturation of the sample with defects increases the proportion of fcc clusters, for which an increased content of boron is preferable. The concentration of defects at point B in Fig. 13 attains a critical value, after which the system loses its stability. The accumulated defects are probably 'dumped' as a result of dynamic recrystallization, due to which the proportion of fcc clusters and the associated boron concentration in the material decrease. The process of accumulation and dumping of defects, accompanied by oscillations in boron concentration, is repeated due to the continued supply of energy. It should be noted that cyclic reactions are quite typical of open systems. A well-known example of such a reaction is the self-oscillating oxidation-reduction regime in the Belousov–Zhabotinsky reaction [255].

A cyclic amorphization–crystallization reaction that proceeds without a change in the chemical composition and, therefore, only due to the evolution of defects during exposure, was observed in the Co–Ti system [53, 256]. Complete or partial amorphization occurs in this alloy as a result of mechanical processing. When the critical concentration of defects is attained, recrystallization occurs, which restores the crystal lattice. The processes of amorphization and recrystallization alternate with each other under conditions of continued exposure, repeating in a cyclic way.

A common feature of the transformations described in this section is the combined effect of competing transformation mechanisms (direct mixing, accumulation and dumping of defects, diffusion in the bulk and at grain boundaries, etc.). This circumstance usually suggests using sufficiently intense exposures at moderate temperatures, when the supplied energy can dissipate in the system through various channels.

The summarize, the two main mechanisms by which nonequilibrium transformations under SPD conditions are implemented should be distinguished. At low temperatures, 'direct mixing' of atoms prevails, while at moderate temperatures, abnormal transformations occur due to diffusion on moving defects (dislocations, grain boundaries). At present, the discussion about the 'relative contribution' of these mechanisms to the overall picture has not been completed. Suppression of the dislocation deformation mode in nanocrystalline samples and the possibility of an interstitial (including crowdion) mechanism of mass transport are important arguments in favor of the diffusive nature of abnormal transformations, even at cryogenic temperatures. The phenomena of abnormal decomposition and the realization of low-temperature phases should be controlled, probably by diffusion along dislocations and grain boundaries. Models based on the concept of the development of transformations due to flows of nonequilibrium vacancies, changes in the thermodynamics of an alloy due to the energy of accumulated defects, and local heating of the material in the process of exposure are apparently of a particular nature and have no significant experimental evidence.

3. Segregations and grain-boundary decomposition in nanocrystalline materials

A nanocrystalline (NC) state of a material is often attained as a result of SPD, in which the proportion of atoms located in the GB region proves to be comparable to their bulk proportion. The grain size becomes in this case an important thermodynamic factor that determines the phase composition of the alloy. The main mechanism that sets the relationship between the grain size and the phase composition is the formation of segregations of impurity and alloying elements on GBs [66, 257–260]. The segregations can significantly change the phase equilibrium of the alloy [261] and the thermal stability of the structure [262, 263]. The role of segregations on GBs is especially significant in NC alloys [1, 264], where the proportions of atoms on GBs and in the grain volume are comparable.

Segregations of alloying components at grain boundaries significantly affect the strength of alloys, facilitate the transition to a nanograined state under SPD (for example, due to segregations of magnesium in aluminum, the attained grain size decreases by an order of magnitude), and stabilize the grain structure in the process of annealing (in alloys of nickel, silver, copper, etc.) [47], while the formation of thin grain boundary layers of zinc at grain boundaries in aluminum after torsion under high pressure facilitates sliding of grain boundaries and leads to high plasticity of ultrafine Al–Zn alloys [49]. It should be noted that understanding segregation effects is of utmost importance for the chemistry of catalysis and the reactivity of solids [265]. The key factor in the models proposed to describe the catalytic properties is segregation effects, the role of which increases with decreasing nanoparticle size [266, 267].

The distribution of components in the NC alloy, which occurs after SPD in the process of annealing at moderate temperatures (in the absence of recrystallization), is described in phenomenological terms by the classical theory of segregations [259, 268], including taking account of the dependence of the impurity concentrations in the bulk and on GBs on the grain size [269–272] and account of the joint segregation of impurities of various types [273–276]. A specific feature of SPD is that segregations can develop in the process of dynamic recrystallization on moving GBs [155, 239, 245–247]. At the same time, the GBs themselves are 'non-equilibrium' and feature significant distortions and a high segregation capacity [3]. It was shown in [269, 271] that there is a critical grain size in dilute alloys, upon attaining which the grain volume is cleared of impurities (Fig. 14a), and the impurity concentration on the GB begins to decrease in comparison with that for larger grains (Fig. 14b).This can lead in multicomponent alloys to a nonmonotonic behavior of the concentration of segregated alloy components as a function of the grain size [271].

It was first predicted in [277] and then confirmed both experimentally [47, 262, 278, 279] and by numerical simulation using the molecular dynamics method [280] that grain boundary segregations (GBSs) stabilize in some systems the grain structure, ensuring that the equilibrium grain size is attained, contrary to the trend of collective recrystallization. According to [277], if the impurity segregation energy is sufficiently high, the presence of a GB in the system may become energetically favorable. The equilibrium grain size attained in this case was estimated in [281, 282], and it was shown in [283] that it rapidly increases with decreasing

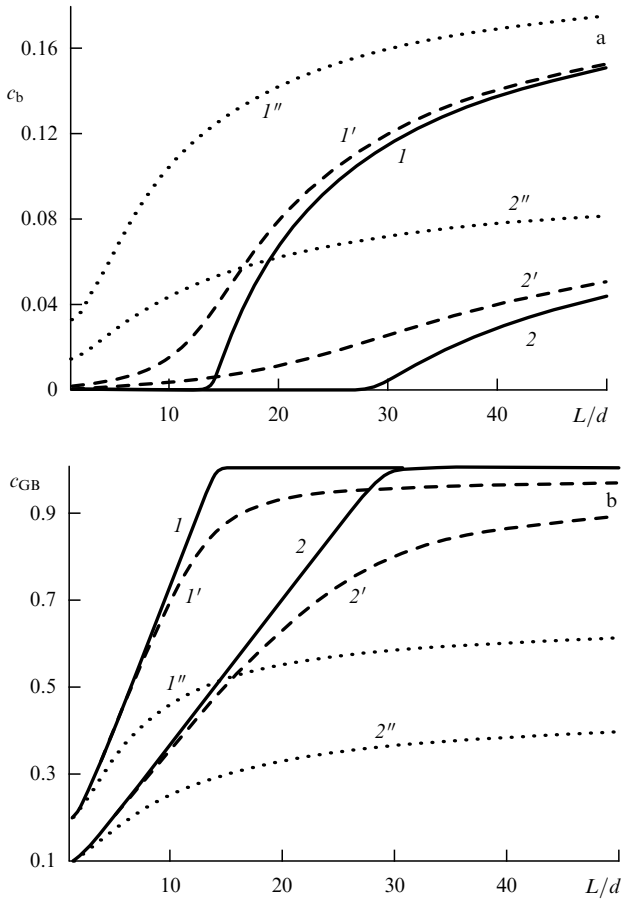

Figure 14. Equilibrium impurity concentration in the bulk (a) c_b and at the boundary c_{GB} (b) of a grain as a function of the grain size at $c_0 = 0.20$ (curves *1*, *1′*, *1″*) and $c_0 = 0.10$ (curves *2*, *2′*, *2″*) at various segregation energies at the boundary: $-\delta\varepsilon_s/(k_B T) = 10$ (curves *1*, *2*), 5 (curves *1′*, *2′*), and 2 (curves *1″*, *2″*) [271].

impurity concentration, theoretical estimates being in good agreement with experimental data for the Ni–P and Ni–W systems. Attention was drawn in [271] to the fact that the grain boundary width d and the grain size L are present in equations that describe segregations in the form of a dimensionless ratio d/L; therefore, for systems in which the Weissmüller effect [198] is realized, an alternative scenario is also possible, in which the equilibrium grain size is not attained, and wide nonequilibrium GBs are formed instead.

GBSs trigger in thermodynamically unstable alloys the development of spinodal decomposition, as was previously demonstrated using the generalized Cahn–Hillard model [284] that takes into account the local change in the chemical potential at the GB [285–288] (Fig. 15a). It has been shown recently using the Monte Carlo method with consideration for lattice relaxation that GBSs trigger the development of discontinuous grain-boundary decomposition in the Fe–Cu system [289] (Fig. 15b). Study [272] provides a classification of the morphological features of the GBSs and grain boundary decomposition as a function of temperature. If temperature decreases, segregations at the GBs can be replaced by the formation of precipitates at triple junctions, followed by grain boundary decomposition over the entire GB area and, finally, by spinodal decomposition in the bulk of grains (Fig. 16).

Unusual ('nonequilibrium') grain boundaries (NGBs) are known to be formed under SPD [3], which are characterized

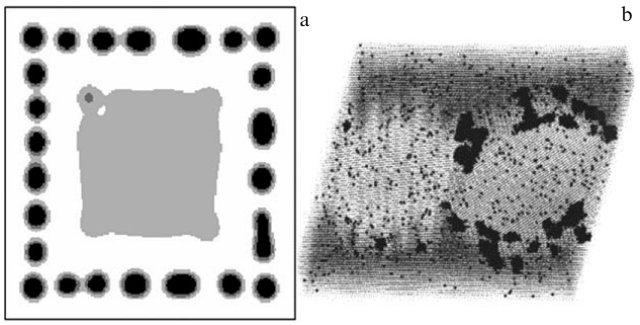

Figure 15. (a) Grain boundaries (coinciding in the simulation of the phase field with the boundaries of the square) trigger the emergence of a chain of equidistant precipitates under spinodal decomposition [285]. (b) Monte Carlo simulation of the decomposition in an Fe–Cu polycrystal [289].

by a high segregation capacity and significant distortions of the crystal lattice in a wide boundary layer. This assertion is supported by experiments [290, 291], which demonstrate a significant structural relaxation of such GBs upon annealing. The phenomenon of grain-boundary wetting was used in [292] to show that unrelaxed grain boundaries have a higher energy after deformation. The first models of NGBs assumed that a wide amorphous layer is formed between crystallites [293]. Subsequent experiments showed that the width of the layer in which the crystallographic coordination is disturbed does not exceed one or two interatomic distances [294]. The magnitude of deformations turns out in this case to be significant (more than 0.1%) in a wide near-boundary region [295, 296], where an increased density of dislocations is observed [3]. It should be noted that the assumption regarding a quasi-amorphous layer between crystallites seems natural near the transition of the alloy to the amorphous state. Expected in this case may be the emergence of unconventional wide GBSs, which should 'dissolve' upon annealing and evolve into conventional (equilibrium) GBSs. This problem is still poorly explored by both theory and experiment.

Another specific feature of SPD is the active migration of GBs during exposure [65]. It was hypothesized in [297] that the kinetics of GBSs formation is restricted in this case not by bulk diffusion, but by the redistribution of alloy components on the GB. The moving GB 'sweeps' the impurity atoms, which leads to the formation of the GBSs directly during the exposure, even at sufficiently low temperatures (~ 300 K). This approach made it possible to interpret the formation of segregations on GBs in the Al–Mg and Al–Zn systems during SPD [297], while the estimated bulk diffusion coefficients (even taking into account their increase due to the generation of nonequilibrium vacancies under SPD) indicate that such a process is not feasible. A simple model of the formation of segregations on moving GBs was proposed in [155] to show that at low T the motion of GBs is a prerequisite for the formation of segregations, and the GBSs attain their maximum value at the optimal velocity of GB motion (see Fig. 17).

Models based on the concept of an alloy moving away from thermodynamic equilibrium under the effect of vacancy [63] or dislocation [227] flows predict that nonequilibrium

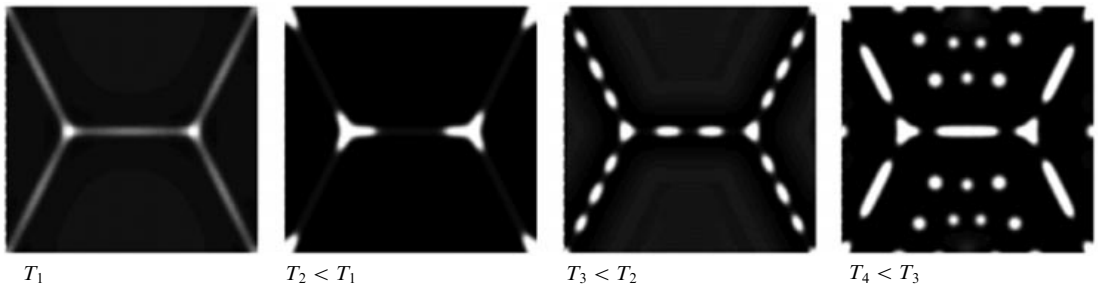

Figure 16. Typical morphologies of grain-boundary segregations and formation of precipitates under exposure at various temperatures [272].

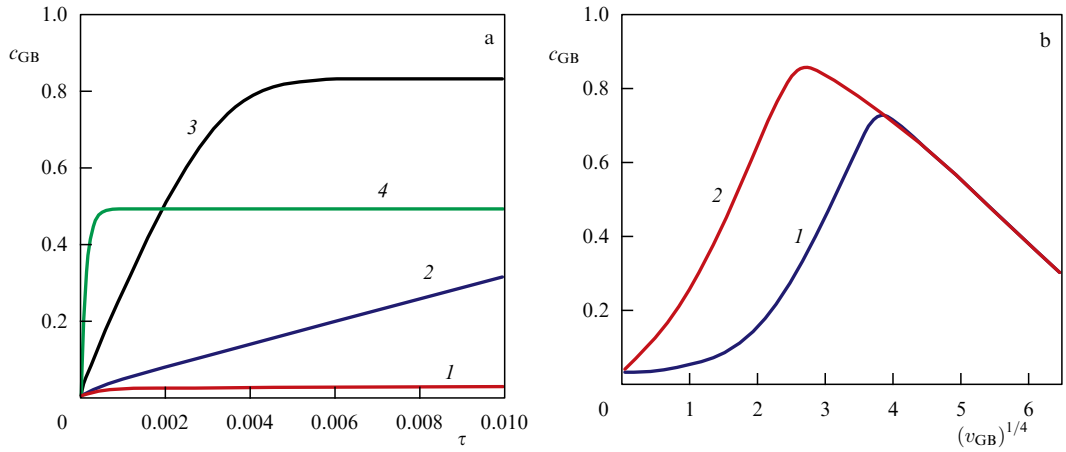

Figure 17. (a) Evolution of the impurity concentration at the grain boundary for the velocity of the boundary motion $v_{GB} = 0$ (curve *1*), 12.5 (curve *2*), 100 (curve *3*), and 800 (curve *4*). (b) Segregation attained by the time $\tau = 0.002$ (curve *1*) and 0.02 (curve *2*) as a function of the velocity of the boundary. The average impurity concentration is $c_0 = 0.01$, the segregation energy is $\delta\varepsilon_{GB} = -0.3$ eV per atom, $T = 500$ K, $D_{GB}/D_{bulk} = 10^5$ [155].

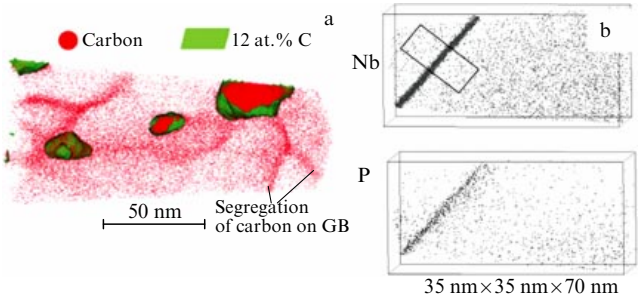

Figure 18. Results of 3D atom probe tomography: (a) segregation of carbon at equilibrium grain boundaries and precipitation of cementite in Fe–4.4C–0.3Mn–0.39Cr–0.21Cr steel (at.%) [45]; (b) segregation of niobium and phosphorus at the large-angle grain boundary in alloyed ferritic steel (Fe–18Cr–0.32Nb–0.045P (at.%)) [46].

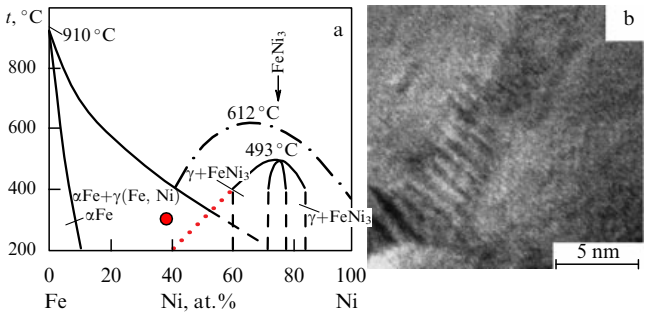

Figure 19. (a) Phase diagram of the Fe-Ni alloy that demonstrates the presence of two-phase regions $\gamma(\mathrm{Fe, Ni}) + \mathrm{FeNi_3}$ poorly studied in the low-temperature region [301]; the decomposition is not observed if the alloy (dot) is processed above the extrapolated boundary of the two-phase region (dashed line) [42]. (b) Signs of decomposition with ordering at the grain boundary in the $\mathrm{Cr_{12}Ni_{30}Fe_{58}}$ (at.%) alloy subjected to SPD at $T = 20\,^{\circ}\mathrm{C}$ [42] detected using electron microscopy.

segregations may be formed under intense exposure, for example, under SPD.

For example, it was hypothesized in [63] that nonequilibrium vacancies are generated at some boundaries and junctions of grains and subsequently sink to other boundaries in the process of SPD. The stratification of the alloy occurs as a result due to the difference in the diffusive mobility of atoms of different types by means of the inverse Kirkendall effect [161, 162]. This concept predicts new physical phenomena, such as the formation of intermediate-composition regions near the source of vacancies and the formation of modulated structures whose period depends on the distance between the source and the sink of vacancies [298, 299]. However, the assumption that the spatial configuration of sources and sinks of vacancies under SPD does not change remained unsubstantiated. If a random variation in this configuration with time or uniform generation of vacancies over the entire surface of grains is assumed, the effects predicted in [298, 299] vanish. They are more likely to be observed under irradiation at moderate temperatures.

We now discuss the experimentally observed scenarios of how segregations and decomposition at grain boundaries are formed. Three-dimensional atom probe tomography was applied in [45] to explore grain-boundary segregations in Fe–4.4C–0.3Mn–0.39Cr–0.21Cr (at.%) steel after cold drawing and subsequent annealing for 2 min at $T = 400\,^{\circ}\mathrm{C}$. The width of the segregations was shown to be as large as several nanometers and depends on disorientation of neighboring crystallites (Fig. 18a). Study [46] discovered 2–3-nm wide segregations of niobium, boron, phosphorus, and molybdenum at large-angle GBs in a complex alloyed steel after hot-rolling deformation (860 °C) (Fig. 18b). The large width of carbon segregations may only be due to structural changes in the crystalline lattice in the GB region. The reason for the emergence of wide segregations in the case of joint segregation of impurities requires further exploration, since the driving force of segregation is, for some alloys (Nb, Mo), interaction with GB, while for others (B, P), it is interaction with other impurities.

An example of grain-boundary decomposition with precipitation of an equilibrium low-temperature phase is the Fe–Ni–Cr system [42]. Field ion microscopy finds after SPD at $T = 20\,^{\circ}\mathrm{C}$ traces of equilibrium $\mathrm{FeNi_3}$ or FeNi phases whose dimensions are ≈ 5 nm, and electron microscopy, ordered-phase domains located in a periodic way along GBs (Fig. 19). A simulation based on molecular dynamics (MD) methods [300] has shown at the same time that equilibrium segregations due to a change in the chemical potential of nickel atoms on the GB are not possible in the Fe–Ni system due to small segregation energies.

The two-phase region γFe(solid solution)+$\mathrm{FeNi_3}$, which is present in the equilibrium phase diagram, is a reflection of the fact that the $\mathrm{FeNi_3}$ intermetallic is formed as a result of a decomposition reaction with ordering in the initial solid FCC solution, i.e., without the formation of αFe [301]. Such a two-phase region may also exist in the vicinity of the FeNi phase [302], which is metastable with respect to decomposition into $\alpha\mathrm{Fe} + \mathrm{FeNi_3}$ and, therefore, is not displayed in standard phase diagrams. The composition of steel selected for study ($\approx 50-60$ at.%) is located precisely in this poorly explored region of the phase diagram. Decomposition has not been observed if the alloy was processed at $T = 300\,^{\circ}\mathrm{C}$, i.e., under conditions above the two-phase region dome. It should be noted that the precipitation of the $\mathrm{FeNi_3}$ or FeNi phases may be accelerated as a result of segregations stimulated by the flow of point defects on the GB [300].

Grain-boundary decomposition is also realized in the $\mathrm{Al_{94}Mg_6}$ alloy subjected to SPD in the two-phase region [47], where a layer enriched in magnesium up to 10 nm thick emerges along the GB (Fig. 20). The equilibrium $\mathrm{Al_3Mg_2}$ phase is known to rapidly precipitate in aluminum on grain boundaries, a problem which is of importance for technology [303]. However, X-ray diffraction analysis has failed to reveal in this case the presence of an ordered phase. Recent experimental and theoretical studies [304] have shown that decomposition in the Al–0.94Mg–0.47Si alloy below the two-phase region dome begins in a solid fcc solution, and clusters enriched in both silicon and magnesium are observed, whence it follows that the mixing energy of the components in the solid solution is negative, $v < 0$. However, ab initio calculations [228] resulted in the opposite conclusion, $v > 0$; therefore, the mechanism of the initial stages of decomposition in the Al–Mg system currently remains unclear. It is also necessary to bear in mind the possible competition between two processes: the precipitation of the equilibrium $\mathrm{Al_3Mg_2}$ phase and its disordering under the effect of SPD [297].

The alloy NH-7075, of a similar composition ($\mathrm{Al_{93.6}Zn_{2.55}Mg_{2.89}Cu_{0.61}Si_{0.11}Cr_{0.10}Ti_{0.01}}$), subjected to SPD by means of torsion under pressure at $T = 200\,^{\circ}\mathrm{C}$ was

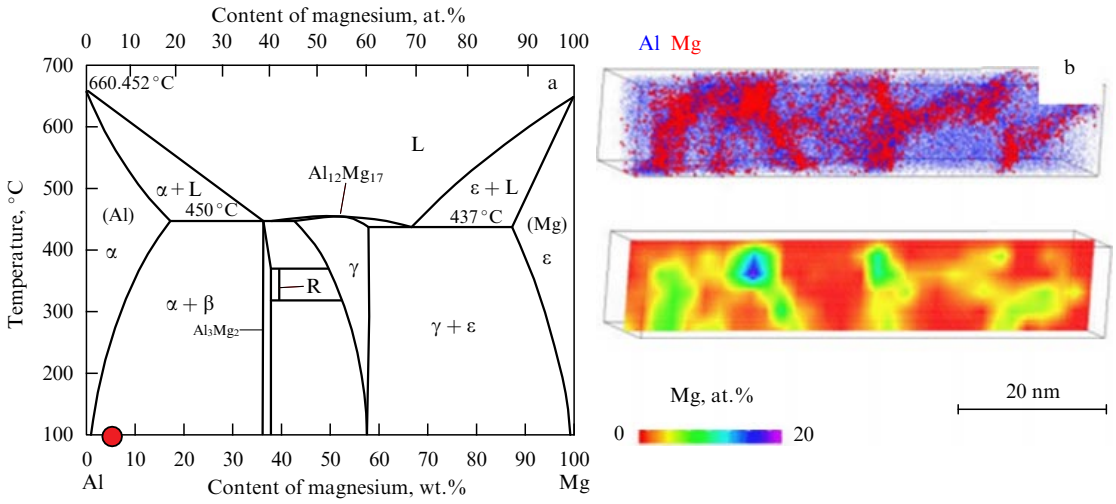

Figure 20. (a) Phase diagram of the Al–Mg alloy; the dot indicates experimental conditions [47] below the boundary of the two-phase Al + Al_3Mg_2 region. (b) Grain-boundary decomposition in a solid solution subjected to SPD [47] visualized using atom probe tomography.

investigated in [48]. X-ray structural analysis showed that the alloy after exposure is in the state of a solid fcc-solution without signs of intermetallic phases. Atom probe tomography revealed needle-shaped precipitates (width ≈ 4 nm, length ≈ 18 nm) of a mixed Mg + Zn + Cu composition on some small-angle GBs and spherical precipitates ≈ 4 nm in diameter at some triple grain junctions. The state of the alloy in the bulk of grains was characterized in this case by a strong short-range order (clustering of impurities), although the alloy parameters are located under normal conditions slightly above the two-phase region dome. The authors of Ref. [297] have shown that the factor responsible for the decomposition may be in this case the applied pressure that displaces the phase-diagram point of the alloy in the diagram below the two-phase region dome.

In the αFe–9 wt.% Mn alloy after holding at moderate temperatures the wide segregations are also found [305], apparently associated with decomposition into GBs, since the mixing energy of the components in the solid solution is in this system negative, $v < 0$ [306].

Abnormal stratification after crushing of $Ni_{41}Pd_{59}$ alloy powder in a ball mill [307] was observed by determining the shift in the Curie temperature (Fig. 21), which had the maximum value after processing at a moderate temperature (403 K). If the alloy was processed at higher (523 K) or lower (80 K) temperatures, stratification was barely observed.

However, decomposition developed in the process of annealing at $T = 553$ K after low-temperature SPD. Since the Ni–Pd system forms a continuous series of solid solutions ($v > 0$), the decomposition with the precipitation of equilibrium phases is in this system thermodynamically infeasible. Owing to the significant magnitude of the effect, the stratification apparently cannot be associated with equilibrium grain boundary segregations. Effects of this type may be caused, for example, by the formation of segregations on wide nonequilibrium GBs or under the effect of nonequilibrium-vacancy flows [63].

To sum up, it should be noted that the formation of GBSs undoubtedly plays a significant role in phase equilibrium and the development of transformations in nanocrystalline materials obtained in low-temperature SPD with subsequent annealing at moderate temperatures.

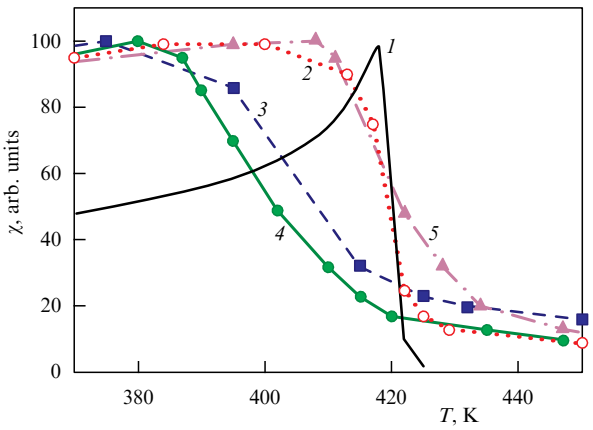

Figure 21. Magnetic susceptibility of the $Ni_{40}Pd_{60}$ alloy before (curve *1*) and after processing in a ball mill at temperatures of 80 K (curve *2*), 300 K (curve *3*), 403 K (curve *4*), and 523 K (curve *5*) [307].

The theory of equilibrium GBSs is currently well developed and its generalizations for the case of nanocrystalline materials have been proposed. However, experiments often indicate that GBSs develop directly in the process of plastic deformation (nonequilibrium segregations) even at room temperature, when bulk diffusion is frozen. These observations may be explained by using the concept [155] of GBSs formation on moving GBs (see Fig. 17), when accelerated mass transport is provided by grain boundary diffusion.

4. Problem of abnormal diffusion under intense plastic deformation

The role of diffusion in the realization of nonequilibrium phase transformations under SPD remains a matter of discussion. The rate of transformation in substitutional alloys under SPD is 10–20 orders of magnitude higher than the conventional one [43, 81, 151, 308], and the dissolution of intermetallic particles occurs even at temperatures of ~ 100 K [32, 230], at which not only bulk diffusion but also diffusion along dislocation tubes is considered to be frozen. Therefore, direct mechanical mixing remains the most common explanation for these transformations [14, 58].

However, not only mechanical alloying under SPD at room temperature, but also decomposition with the precipitation of low-temperature equilibrium phases (for example, in the Cu–Co system [151]), nonequilibrium phases (for example, the reaction $Nd_2Fe_{14}B \rightarrow$ amorphous phase $+\alpha Fe$ [158]), and abnormal stratification in the system of well miscible Ni–Pd components [307] have been observed. These transformations, which indicate precisely the anomalously high rate of diffusive mass transfer, stimulated the exploration of the role of diffusion in the disordering of alloys and the formation of supersaturated solid solutions, i.e., in those phase transformations that are typical of SPD but are often considered to be diffusionless.

It has been hypothesized in [63] that diffusion is accelerated under SPD due to the generation of a large number of nonequilibrium vacancies at grain boundaries and triple junctions. A typical concentration of vacancies in a material during SPD is $10^{-4}-10^{-5}$ [70–74], values that correspond to the pre-melting state. It may be expected in this case that the bulk diffusion coefficient at $T \sim 300-400$ K will increase by 5–10 orders of magnitude or more (depending on the material) [309, 310]. However, in the opinion of many authors [32, 311], this is insufficient for nonequilibrium transformations to develop within the observed timeframes. Therefore, it must be assumed that not only the pre-exponential factor but also the diffusion activation energy changes. It was suggested in [312] that the supersaturated solution is formed in the Fe–Cu system as a result of diffusion through dislocation tubes, while in [238] it was assumed that the crowdion mechanism of diffusion at dislocations ensures mass transfer, even at $T = 77$ K.

In our opinion, special attention should be paid to the role of grain-boundary diffusion, which is additionally accelerated by 3 to 5 orders of magnitude when nonequilibrium GBs are realized [313], and also due to the generation of nonequilibrium point defects under SPD [63]. In has been shown in recent study [155] that the diffusion on moving GBs may result in a variety of nonequilibrium phase transformations, including disordering of the alloy and dissolution of precipitates.

Figure 22 shows the coefficients of bulk (curve *1*), dislocation (curve *2*), and grain boundary (curve *3*) diffusion for the Fe–Cu and Ag–Cu system extrapolated to the low temperature region using published data [314–318]. The transformation can be carried out in reasonable times of ~ 10 s [173, 311] by means of one of the mechanisms listed above, provided that the corresponding diffusion coefficient is higher than the level of line *4* in Fig. 22.

It can be seen that an increase in the bulk diffusion coefficient D_{bulk} by 10 orders of magnitude due to the generation of nonequilibrium vacancies under SPD is insufficient for the occurrence of transformations at room temperatures (curve *1′*).

A large spread of estimated D_{bulk} values should be noted. The estimated equilibrium density of vacancies in copper at $T = 300$ K varies from 10^{-12} [319] to 10^{-15} at a vacancy formation energy of 0.87 eV [320]. The density of vacancies under SPD is as high as 10^{-5} [173] to 4×10^{-4} [319]. As a result, an increase in D_{bulk} under SPD by 7–11 orders of magnitude should be expected.

If an assumption is made that phase transformations are controlled by grain boundary diffusion, then, as Fig. 22 shows, the diffusion rate required for the realization of transformations at $T \sim 300$ K is not attained either (curve *3*). Given that diffusion on nonequilibrium GBs increases by 3–5 orders of magnitude [313], the realization of diffusion-controlled transformations turns out to be possible at $T \sim 400$ K.

The conclusions of [313] on the acceleration of diffusion on nonequilibrium GBs refer to *after*-SPD samples. It is reasonable to assume that the grain boundary diffusion is additionally accelerated in SPD along with bulk diffusion due to the generation of nonequilibrium point defects [63]. Curve *3″* in Fig. 22, which corresponds to this case, already allows the realization of diffusion transformations at $T \sim 300$ K.

As noted in [59], although formally the rate of abnormal mechanical alloying under SPD can indeed be ensured due to grain-boundary diffusion, the physical mechanism due to which diffusion could move the system away from thermodynamic equilibrium is unclear. According to [155], such a mechanism can be provided by the migration of GBs and 'freezing' of the attained nonequilibrium state behind the GBs.

Study [81] investigated the abnormally fast decomposition in Al–Mg and Al–Zn–Mg alloys during SPD by torsion under a pressure of 5 GPa at $T = 300$ K. As a result of the decomposition, precipitates of the Al_3Mg_2 and $Mg_{32}(ZnAl)_{49}$ phases with a size of ≈ 10 nm were formed, which are uniformly distributed over the bulk of the material. Estimates [81] made under the assumption that the transformation is controlled by bulk diffusion show that the increase in

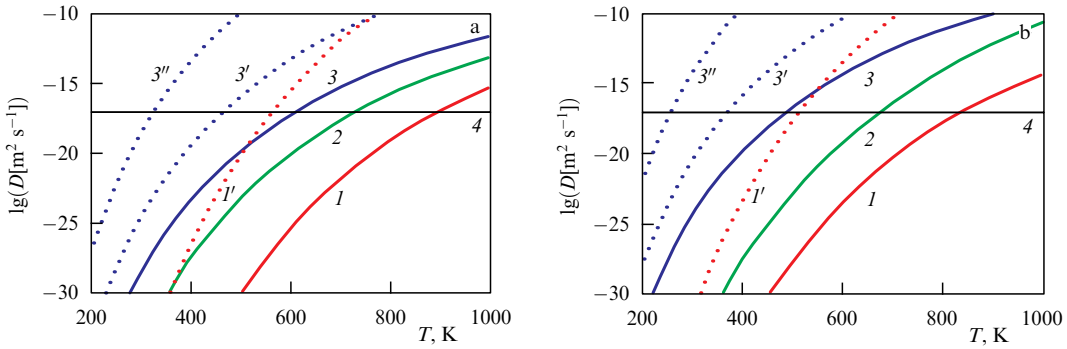

Figure 22. Coefficients of bulk D_{bulk} (curve *1*), dislocation D_{disl} (curve *2*), and grain-boundary D_{GB} (curve *3*) diffusion in Fe–Cu (a) and Ag–Cu (b) systems extrapolated to the low-temperature region according to [314–318] and estimates of D_{bulk} and D_{GB} taking into account nonequilibrium vacancies (curves *1′* and *3″*, respectively) and D_{GB} taking into account the nonequilibrium state of grain boundaries (curve *3′*). Horizontal straight line *4* corresponds to the diffusion coefficient that ensures the transport of atoms over a distance of ~ 10 nm within a time of ~ 10 s.

the diffusion coefficient upon SPD, $D_{\text{bulk}}^{\text{HPT}}/D_{\text{bulk}}$, was 8–9 orders of magnitude. If it is assumed that the transformation is controlled by grain boundary diffusion, the $D_{\text{GB}}^{\text{HPT}}/D_{\text{GB}}$ ratio will be 3–5 orders of magnitude. An applied pressure of 5 GPa further lowers in this case the diffusion rate in these alloys by three to five orders of magnitude [297]. Therefore, the most probable mechanism of decomposition is grain boundary diffusion (on moving GBs) accelerated due to the generation of nonequilibrium vacancies [81].

Abnormally fast decomposition in the Cu–Ni system was studied under the same conditions in [43]. Even if the generation of nonequilibrium vacancies is taken into account, the estimated ratio $D_{\text{bulk}}^{\text{HPT}}/D_{\text{bulk}}$ was 6–10 orders of magnitude [43], and it should be even higher if the applied pressure is taken into account. If the transformation is controlled by grain boundary diffusion, the $D_{\text{GB}}^{\text{HPT}}/D_{\text{GB}}$ ratio is about three orders of magnitude. Thus, the experimental observations support the hypothesis regarding the decisive role of grain-boundary diffusion (on moving GBs) in the processes of abnormally accelerated decomposition.

In discussing the abnormally high rate of diffusive mass transfer under SPD, the interstitial diffusion mechanism is often mentioned [32, 68, 238, 321]. The generation of interstitial defects on vacancy sinks as the temperature decreases and the critical stress is attained was hypothesized for the first time in [322, 323] and experimentally confirmed in [324]. Therefore, it was believed for some time that interstitial defects can provide mass transfer at low temperatures [325]; however, theoretical estimates [326] have cast doubt on this mechanism. It is argued in [69] that there is no evidence of diffusion over interstices for any of the metallic systems. However, based on the change in the average lattice parameter after mechanical treatment of Ni–Ti and Fe–Ni alloys, a conclusion was made in [68] that up to 1 at.% of interstitial atoms are accumulated in the bulk of the material. A computer simulation [327] has shown that the energies of formation of vacancies and interstitial defects at grain boundaries are comparable; therefore, grain-boundary diffusion can, apparently, be implemented by defects of both types.

The performed analysis shows that the phenomena of abnormal stratification and decomposition of alloys at SPD at moderate temperatures can be maintained by diffusion on moving dislocations and GBs, the rate of which additionally increases due to the generation of vacancies and interstitial atoms. Since this mechanism is realized under locally changed thermodynamic conditions, it may also be responsible (at least at temperatures close to room temperature) for the implementation of those transformations that are often considered diffusionless (disordering, mechanical alloying).

5. Classification of phase transformations under severe plastic deformation

The variety of possible types of transformations upon SPD is apparently explained by the effect of various mechanisms (direct mixing, anomalous diffusion on moving defects, development of grain-boundary segregations), which were discussed above. An approach was proposed in [328] to systematize the diversity of experimental facts by using the concept of changes in the microscopic mechanisms of transformations that depend on external conditions (temperature and treatment intensity). The main provisions of this concept with minor clarifications are presented below.

The mechanical energy supplied to the system is partially converted in the process of plastic deformation into heat and partially accumulated at the grain boundaries and junctions in the form of elastic energy of mesodefects formed due to the incompatibility of plastic deformation [64, 329, 330]. The emerging nonequilibrium states of the alloy may be considered a result of dissipation of this elastic energy through the available channels of structural relaxation (plastic deformation, amorphization, dynamic recrystallization, generation of nonequilibrium point defects, and diffusive redistribution of alloy components). The conditions for switching between the specified mechanisms of dissipation of elastic energy depend on many factors (temperature, pressure, total strain, strain rate, grain size, etc.). We follow the general principles of nonequilibrium thermodynamics [253, 254], distinguish the rate with which mechanical energy is supplied to the system W as a control parameter. The second important parameter is temperature T that determines the rate of relaxation processes.

The energy W transferred to the system is spent on heat production, generation of defects, and increases the free energy of the alloy:

$$W = \frac{\mathrm{d}H}{\mathrm{d}t} - T\frac{\mathrm{d}S}{\mathrm{d}t} + \frac{\mathrm{d}E_{\text{def}}}{\mathrm{d}t} + q\,, \tag{3}$$

where H and S are the alloy enthalpy and entropy, E_{def} is the energy of defects, and q is the release of heat in the system per unit time. The form of Eqn (3) is more general than that proposed in [65], where only the energy of defects was considered and the change in the values of H and S as a result of the possible development of nonequilibrium transformations was not taken into account. The steady state of the alloy achieved after prolonged treatment is characterized by nonequilibrium stationary values $H(T, W)$, $S(T, W)$, $E_{\text{def}}(T, W)$, and the flow of supplied energy is completely converted into heat ($W = q$). Thus, under SPD conditions, the alloy is a classical dissipative system [253, 254].

Figure 23 schematically shows a diagram of nonequilibrium stationary states of the alloy in the homologous temperature (T/T_{m}) coordinates — the intensity of external action (W). The characteristic lines of the diagram are drawn conventionally, but in qualitative agreement with the experimental facts.

Equilibrium or nonequilibrium phase transformations are realized in the alloy in the process of plastic deformation due to the competition between the energy accumulation and dissipation. Depending on the rate of relaxation processes that return the alloy to thermodynamic equilibrium, areas which differ in the behavior of the alloy under an external effect may be distinguished in the diagram.

At high temperatures, when relaxation processes are sufficiently quick (sector I), equilibrium phases are realized in the system. Sector I is bounded at the top by a line above which an external action violates thermodynamic equilibrium, and on the left by a line (1) of 'freezing' of bulk long-distance diffusion, which is necessary for phase transformations with a change in chemical composition during characteristic times of external action. It is generally accepted that bulk diffusion can be disregarded under normal conditions if $T/T_{\text{m}} < 0.5$. Line (1) has a negative slope because SPD accelerates diffusion by 5–15 orders of magnitude due to the generation of nonequilibrium point defects (see Section 4). Therefore, low-temperature phases may be realized during external action, which are difficult to attain using other

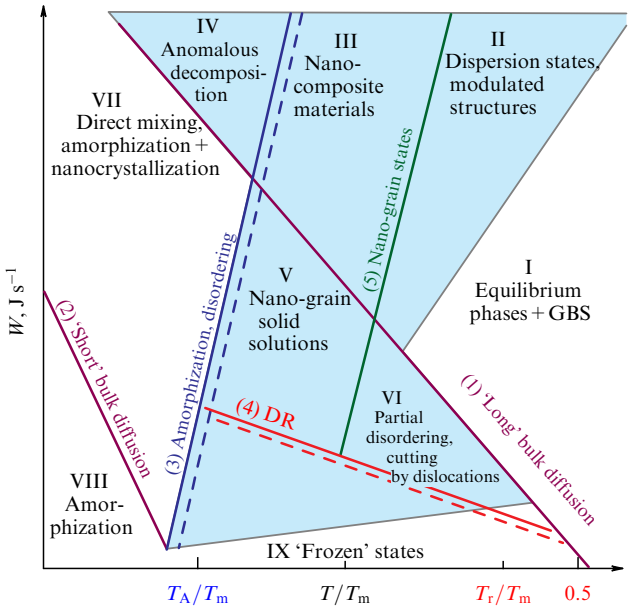

Figure 23. Diagram of nonequilibrium stationary states of the alloy under SPD conditions. The region of nonequilibrium diffusive phase transformations is shaded. (See details in the text.)

processing methods. In particular, it was possible to observe even at room temperature decomposition with the precipitation of equilibrium phases in such systems as Ni–Cu [41, 43], Cu–Co [151], and Fe–Ni [42]. The accelerated formation of particles of the equilibrium Ni_3Al phase was observed in the Fe–Ni–Al alloy as a result of SPD in Bridgman anvils at $T = 573$ K, while the treatment at $T = 77-473$ K resulted, on the contrary, in the dissolution of such precipitates [331].

The external influence (deformation) effectively competes at moderate temperatures with relaxation processes, leading to a variety of nonequilibrium phase and structural states (sectors II–VI). These states differ by the way of dissipation of the energy supplied to the alloy. The region of nonequilibrium diffusive phase transformations is shaded in Fig. 23; a detailed description of these sectors is given below.

At low temperatures, when diffusion processes are suppressed (sectors VII and VIII), the main modes of dissipation of the energy supplied to the alloy are direct mechanical mixing of the alloy components and amorphization. Disordering and/or amorphization develop to the left of line (3); below line (2), 'short' diffusion, which controls atomic ordering, freezes. According to [9], amorphization occurs when the critical degree of mechanically induced disordering is attained provided that the amorphous state of the alloy is energetically advantageous compared to the disordered state. In the limit of weak external influence (deformation), line (3) attains a temperature of T_A (~ 300 K), at which short-distance diffusion can be ignored. At $T < T_A$, even a relatively weak but long-term plastic deformation can cause complete disordering of the alloy and thereby trigger its possible amorphization. As the grain size decreases, line (3) shifts towards higher temperatures (parallel dashed line), because the high density of grain boundaries facilitates amorphization.

It should be noted that competition between amorphization and 'short' diffusion is possible in sector VII; the latter mechanism performs as an additional driver for returning to an equilibrium (ordered) state and leads to nanocrystallization in the amorphous matrix. This sector includes, in particular, the cyclic amorphization–nanocrystallization reaction observed in the Co–Ti system [53, 256]. In sector VIII, diffusion is completely 'frozen', which prevents, among other things, the development of dynamic recrystallization. It should be expected that plastic deformation in this sector occurs before the onset of amorphization due to the passage of dislocations through the volume of grains, which leads to disordering of the alloy by the direct mixing mechanism [14]. Most of the experimental observations concerning the amorphization of alloys under SPD refer to temperatures no higher than room temperature [8, 9], and a high processing intensity and the attainment of a small grain size are usually not required (sector VIII).

The issue of whether for nonequilibrium transformations upon SPD (with prolonged exposure) to occur a certain threshold of exposure intensity should be exceeded is currently a matter of discussion. It was noted in [174] that the degree of mixing of the components in the Fe–Cu alloy at $T = 77-300$ K is determined by the total, or actual, strain and does not depend on the strain rate. An opinion has been set forth in [65] that abnormal transformations are realized in large ('megaplastic') deformations, regardless of the intensity of alloy processing. This concept is valid, apparently, in the case of low temperatures, when relaxation processes are completely suppressed in the alloy. In our opinion, at higher temperatures and a rather low intensity of external influence (deformation), the energy supplied to the alloy can completely dissipate without the implementation of nonequilibrium phase transformations. Therefore, we distinguish sector IX in the diagram, in which the state of the alloy remains 'frozen'.

The diagram also displays line (4) where dynamic recrystallization (DR) begins and line (5) that separates the regions of nano- and polycrystalline states. Line (4) has a negative slope [65]. For example, DR is observed in the Fe–Cu system under high-pressure shear deformation even at $T = 77$ K [174]. The DR temperature tends in the limit of weak external influence (deformation) to that of the onset of static recrystallization T_r, which, depending on the composition of the material and the magnitude of deformation, may be either lower or slightly higher than $0.5T_m$. As the grain size diminishes, temperature T_r and, consequently, the initial DR line are shifted to the left (dashed line). A concept was proposed in [65], according to which low-temperature DR plays an important role as a mechanism that provides the transition to the nanocrystalline (NC) state, since the conventional mechanisms of plastic deformation (dislocation and rotation modes) degenerate if the grain size decreases to 200 nm [165]. Line (4) DR ends when the line of the onset of amorphization is attained (3), since there is no DR in the amorphous state.

One of the channels through which the energy supplied to the system dissipates is the refinement of the grain structure. A hypothesis regarding the existence of a stationary grain size, which depends on temperature and strain rate, was put forward long ago [332]. Apparently, it has been confirmed experimentally [77, 86, 92–95, 333] (see Section 2.1), which allows drawing line (5). The nanocrystalline state is qualitatively different from the polycrystalline one: the dislocation and disclination regimes of plasticity are no longer operative [64] and nonequilibrium grain boundaries emerge [3], near which the crystal structure of the material is strongly distorted. The positive slope of line (5) reflects the experi-

mental observation that at low temperatures for the transition to the NC state to occur sufficiently large degrees of plastic deformation (duration of external influence) are required, while a high intensity of external influence (deformation) is not needed [65]. Line (5) ends upon reaching initial DR line (4), in line with concept [65], according to which a low-temperature DR is a prerequisite for the transition to the NC state.

We now discuss in detail the nonequilibrium phase transformations controlled by diffusion (shaded area in Fig. 23, sectors II–VI).

In sector II, the mechanisms of nonequilibrium transformations (direct mechanical mixing of atoms, anomalous diffusion at dislocations and GBs) effectively compete with 'long' bulk diffusion, which returns the system to thermodynamic equilibrium. As a result, stationary dispersed states and modulated structures can form (see Section 2.3). For example, modulated structures have been observed in the Ag–Cu system under SPD at higher temperatures ($T > 450$ K), while at lower temperatures a homogeneous state has been attained [30]. The dispersed structure of the precipitates was obtained as the limiting state upon grinding the powder of the FeCr alloy in a ball mill, regardless of whether the initial state was either homogeneous or a mixture of pure components [334].

In sector III, the NC state is attained under conditions of a high rate of bulk diffusion. The formation of nanocomposite materials can be expected in this case in systems that consist of immiscible components. The states attainable can be qualitatively similar to the ones realized in sector II, the difference being that the transition to a dispersed state is now due to the very fact of grain refinement.

In sector IV, the joint development of disordering and 'long' diffusion is possible, providing transformations in which chemical composition changes. The realization of a disordered state in this case assumes a high intensity of processing, since even a 'short' diffusion is sufficient to restore atomic order upon weak external influence (deformation). The disordered state can then undergo a transition to the amorphous phase [9]. The conditions of thermodynamic equilibrium change in the presence of the amorphous phase, which in turn can be accompanied by decomposition with the precipitation of anomalous (nonequilibrium) crystalline phases. An example of such a transformation is the decomposition of the equilibrium tetragonal $Nd_2Fe_{14}B$ phase into an amorphous phase enriched in neodymium and αFe nanocrystals, which was observed at HPT at 5–11 GPa [157]. Also, the phase composition of the final product and the presence of carbides in it were apparently determined in the process of mechanical alloying of a mixture of iron, chromium, and graphite powders in a ball mill by the dynamic equilibrium between crystalline and amorphous phases [335]. Another example is the $Fe_{50}B_{50}$ system, in which the FeB intermetallic compound is realized in the equilibrium state. Various nonequilibrium phases based on iron and boron and an amorphous Fe–B phase were observed in the case of a high intensity of processing of a mixture of iron and boron powders in a ball mill [336]. If the intensity of processing in the same system decreases, a disordered Fe–B solid solution emerges [54, 337]. The transition between two variants of nonequilibrium states in this system should correspond to the shift of the phase-diagram point of the compound from sector IV to sector V in the diagram displayed in Fig. 23.

Probably, sector IV should also include reduction reactions of oxides [20, 21] under SPD, in the process of which oxygen atoms diffuse over long distances, reach the surface, and leave the particle. The occurrence of such reactions indicates that the decomposition of the oxide with the removal of oxygen is more energetically advantageous than the disordered state, which is realized as a result of SPD.

In sectors V and VI, bulk diffusion is suppressed, while the condition for the onset of amorphization has not been fulfilled. It may be expected in this case that nonequilibrium phase transformations are realized due to diffusion at dislocations and grain boundaries, which move in the process of external influence (deformation) [155]. According to concept [65], plastic deformation in the NC state (sector V) occurs due to the migration of grain boundaries, while the leading plasticity mode in the polycrystalline state (sector VI) is dislocation slip [64]. The difference between the mechanisms of plastic deformation in these sectors may be the reason for the difference between the phase transformation scenarios.

In sector V, diffusion along grain boundaries is of significance, owing to which the development of nonequilibrium segregations or decomposition on GBs may be expected. Experimental data show that the phenomenon most frequently observed in this sector of the diagram is the formation of supersaturated solid solutions in the process of mechanical alloying [13], which may indicate the important role of grain boundary sliding and dynamic recrystallization in this process. It should be noted that the formation of segregations inhibits DR, thus contributing to the refinement of the grain structure.

In sector VI, diffusion along dislocations, which can be quite mobile, is allowed. Consequently, conditions arise for the local dissolution of precipitates in the process of their interaction with dislocations [32, 60, 155]. Diffusive cutting by dislocations of Ni_3Al γ'-particles in the 75Ni–19Cr–6Al alloy (at.%) [218], intermetallic particles in the Fe–Ni–Ti austenitic alloy [231], and carbides in steels [232] has been experimentally observed. If external influence (deformation) continues for a long time, mechanical alloying may be expected according to the mechanism proposed in [14], due to the refinement of phase precipitates as a result of multiple shears. However, mechanical alloying is activated in most cases [13] in the process of the transition to the NC state (sector V), where the dislocation mode of plasticity is suppressed [64], which is inconsistent with the concept of mechanical alloying proposed in [14]. The latter may be an indication that a more important role is played in these processes by the migration of grain boundaries, since, according to [65], dynamic recrystallization is a prerequisite for the transition to the NC state. Mechanical alloying can be realized in the process of grain boundary sliding or as a result of dissolution of precipitates under locally changed thermodynamic conditions at GBs [155].

We now illustrate the formulated concept of nonequilibrium transformations under SPD using as an example the Mn–Al–C alloy. This system has been extensively studied in experiments at various temperatures and intensity of processing in a ball mill [338–340]. Metastable ordered phase τ is formed near the equiatomic composition in this alloy upon cooling to $T < 840\,^{\circ}$C, which corresponds to a local minimum of free energy. This phase can subsequently decompose with the formation of equilibrium phases enriched in aluminum or manganese.

The τ-phase remained stable at a high temperature $T = 700\,^{\circ}\mathrm{C}$ and a low intensity of external influence (deformation), i.e., metastable equilibrium was maintained, which corresponds to sector I of the diagram. As the intensity of processing increased at the same temperature, decomposition into equilibrium phases $\beta\mathrm{Mn} + \mathrm{MnAl\text{-}r}(\gamma_2)$ was observed, which was apparently triggered by an increase in the density of defects; this phenomenon may be interpreted as a shift from sector I to sector II of the displayed diagram. A similar scenario was observed when the temperature dropped to $500\,^{\circ}\mathrm{C}$.

If the alloy was processed in a ball mill at room temperature ($T = 20\,^{\circ}\mathrm{C}$), the composition of the τ-phase remained stable, which indicates that bulk diffusion is frozen under these conditions. However, disordering of the τ-phase occurred, apparently due to the slip of dislocations through the grain volume (sector VI of the diagram). Finally, processing at 77 K resulted in amorphization (sector VIII), which indicates the absence at these temperatures of any other channel for dissipation of the supplied energy. The absence of amorphization at $T = 20\,^{\circ}\mathrm{C}$ is apparently explained by the effect of the mechanisms that restore atomic or crystalline orders that are fully degenerated at $T = 77$ K.

Thus, the concept proposed in [328] systematizes the results of experimental studies. In addition, an analysis of the experimental results for MnAl shows that the temperature conditions for disordering and amorphization do not always coincide, in contrast to the conclusions made in [9].

6. Conclusion

The attractiveness of using SPD for production purposes is due to the realization of nonequilibrium (or unattainable using alternative processing methods) states of an alloy, which are 'frozen' upon completion of external influence (deformation). Direct mixing of atoms [14, 58], which probably prevails at low temperatures, and anomalous diffusion in the region of structural defects (dislocations, grain boundaries) at moderate temperatures [32, 60, 155] may be distinguished among many discussed mechanisms of nonequilibrium transformations. However, the concepts of transformations caused by flows of nonequilibrium vacancies, changes in the thermodynamics of the alloy due to the energy of accumulated defects, and local heating of the material in the course of exposure are apparently of a particular nature and do not have significant experimental evidence to support them.

Martin's phenomenology [149], which predicts a shift to the high-temperature region of the phase diagram due to the 'ballistic' jumps of atoms in the process of external influence (deformation), is in good agreement with the experimental data at low T. However, the microscopic mechanism of transformation remains in this case a matter of discussion, since the slip of dislocations under SPD is suppressed in the volume of grains during the transition to the nanocrystalline state [64], which contradicts the model of direct mixing [14, 58]. Direct mixing of atoms possibly occurs at grain boundaries in the course of grain boundary sliding and low-temperature dynamic recrystallization, especially since, according to [65], DR is a prerequisite for a nanocrystalline state to be realized.

To analyze nonequilibrium transformations at moderate values of T, a model has been proposed [155] which takes into account diffusion under locally changed thermodynamic conditions at dislocations and grain boundaries and possible migration of boundaries in the process of external influence (deformation). It has been shown that diffusion on moving defects may result, depending on the type of system, temperature, and defect passage rate, in a variety of nonequilibrium structural states and phase transformations (disordering of the alloy, dissolution of precipitates, realization of nonequilibrium phases and dissipative structures, nonequilibrium segregations). The possibility of extending the model concepts of [155] to the low-temperature region is limited by the suppression of diffusion at defects at low T. However, a hypothesis has been put forward in recent work [238] regarding the crowdion mechanism of diffusion at dislocations under SPD, which can maintain diffusive mass transport even at cryogenic temperatures.

A classification of possible scenarios of nonequilibrium transformations under SPD has been proposed based on an analysis of experimental observations and general principles of nonequilibrium thermodynamics. According to the concepts formulated in [328], the change in the transformation mechanism is determined by switching between the channels through which the supplied energy dissipates (diffusion in the bulk of the material and at defects, dynamic recrystallization, and slip of dislocations) as temperature and intensity of external influence (deformation) vary and grain size decreases. A diagram of nonequilibrium stationary states of an alloy during SPD has been proposed, which provides a unified explanation of the set of experimental observations, designates the areas where various models of nonequilibrium transformations are applicable, and predicts the mechanism that drives the development of phase or structural instability as the intensity of external influence (deformation) or temperature change.

The work was performed as part of the Governmental Contract on the topics Magnet (no. AAAA-A18-118020290129-5) and Structure (no. AAAA-A18-118020190116-6), a governmental contract of the Institute of Solid State Physics, Russian Academy of Sciences and the Chernogolovka Research Center, the Russian Academy of Sciences, and the project of the Russian Foundation for Basic Research, no. 18-03-00067.

References

1. Valiev R *Nat. Mater.* **3** 511 (2004)
2. Valiev R Z, Islamgaliev R K, Alexandrov I V *Prog. Mater. Sci.* **45** 103 (2000)
3. Valiev R Z, Aleksandrov I V *Nanostrukturnye Materialy, Poluchennye Intensivnoi Plasticheskoi Deformatsiei* (Nanostructure Materials Obtained by Severe Plastic Deformation) (Moscow: Logos, 2000)
4. Sauvage X, Ivanisenko Y *J. Mater. Sci.* **42** 1615 (2007)
5. Yermakov A Ye et al. *Fiz. Met. Metalloved.* **48** 1180 (1979)
6. Grokhovskaya L G et al. *Phys. Met. Metall.* **64** 127 (1987); *Fiz. Met. Metalloved.* **64** 141 (1987)
7. Korznikov A V et al. *Nanostruct. Mater.* **11** 17 (1999)
8. Yermakov A Ye *Phys. Met. Metallogr.* **72** (5) 1 (1991); *Fiz. Met. Metalloved.* **72** (11) 5 (1991)
9. Bakker H, Zhou G F, Yang H *Prog. Mater. Sci.* **39** 159 (1995)
10. Gialanella S et al. *Acta Mater.* **46** 3305 (1998)
11. Yermakov A Ye, Yurchikov Ye Ye, Barinov V A *Phys. Met. Metallogr.* **52** (6) 50 (1981); *Fiz. Met. Metalloved.* **52** 1184 (1981)
12. Yermakov A Ye, Barinov V A, Yurchikov Ye Ye *Fiz. Met. Metalloved.* **54** 935 (1982)
13. Suryanarayana C *Prog. Mater. Sci.* **46** 1 (2001)
14. Martin G, Bellon P *Solid State Phys.* **50** 189 (1997)
15. Koch C C et al. *Appl. Phys. Lett.* **43** 1017 (1983)
16. Tatyanin Ye V, Kurdyumov V G, Fedorov V B *Phys. Met. Metallogr.* **62** (1) 118 (1986); *Fiz. Met. Metalloved.* **62** (1) 133 (1986)

17. Schwarz R B, Petrich R R, Saw C K *J. Non-Cryst. Solids* **76** 281 (1985)
18. Schwarz R B, Johnson W L *Phys. Rev. Lett.* **51** 415 (1983)
19. Bakker H, Loeff P I, Weeber A W *Def. Diff. Forum* **66–69** 1169 (1989)
20. Bridgman P W *Proc. Am. Acad. Arts Sci.* **71** 387 (1937)
21. Vereshchagin L F, Zubova E V, Burgina K P *Dokl. Akad. Nauk SSSR* **196** 817 (1971)
22. Neverov V V, Burov V N, Zhitnikov P P *Izv. Sib. Otd. Akad. Nauk SSSR Ser. Khim. Nauki* **5** (12) 54 (1983)
23. Benjamin J S *Sci. Am.* **234** (5) 40 (1976)
24. Koch C C, in *Materials Science and Technology*: *A Comprehensive Treatment* (Eds R W Cahn, P Haasen, E J Kramer) Vol. 15 *Processing of Metals and Alloys* (Ed. R W Cahn) (Weinheim: Wiley-VCH, 1991) p. 193
25. Lü L, Lai M O *Mechanical Alloying* (Boston, MA: Kluwer Academic, 1998)
26. Yavari A R, Desré P J, Benameur T *Phys. Rev. Let.* **68** 2235 (1992)
27. Bansal C et al. *J. Appl. Phys.* **76** 5961 (1994)
28. Straumal B B et al. *J. Alloys Comp.* **707** 20 (2017)
29. Wu F et al. *Acta Mater.* **49** 453 (2001)
30. Wu F et al. *Acta Mater.* **54** 2605 (2006)
31. Sagaradze V V, Shabashov V A *Nanostruct. Mater.* **9** 681 (1997)
32. Sagaradze V V, Shabashov V A *Phys. Met. Metallogr.* **112** 146 (2011); *Fiz. Met. Metalloved.* **112** 155 (2011)
33. Shabashov V A et al. *Phys. Met. Metallogr.* **98** 580 (2004); *Fiz. Met. Metalloved.* **98** (6) 38 (2004)
34. Sagaradze V V et al. *J. Nucl. Mater.* **295** 265 (2001)
35. Kimura Y et al. *ISIJ Int.* **39** 176 (1999)
36. Gavrilyuk V G *Raspredelenie Ugleroda v Stali* (Distribution of Carbon in Steel) (Kyiv: Naukova Dumka, 1987)
37. Gavriljuk V G *Mater. Sci. Eng. A* **345** 81 (2003)
38. Shabashov V A et al. *Bull. Russ. Acad. Sci. Phys.* **74** 363 (2010); *Izv. Ross. Akad. Nauk Ser. Fiz.* **74** 393 (2010)
39. Shabashov V A et al. *Phys. Met. Metallogr.* **115** 392 (2014); *Fiz. Met. Metalloved.* **115** 419 (2014)
40. Delcroix P et al. *Mater. Sci. Forum.* **360–362** 329 (2001)
41. Korolev A V et al. *Fiz. Met. Metalloved.* **79** 2 43 (1995)
42. Deryagin A I et al. *Phys. Met. Metallogr.* **106** 291 (2008); *Fiz. Met. Metalloved.* **106** 301 (2008)
43. Straumal B B et al. *J. Mater. Sci.* **47** 360 (2012)
44. Li Y J et al. *Acta Mater.* **60** 4005 (2012)
45. Herbig M et al. *Phys. Rev. Lett.* **112** 126103 (2014)
46. Takahashi J et al. *Acta Mater.* **107** 415 (2016)
47. Sauvage X et al. *Adv. Eng. Mater.* **14** 968 (2012)
48. Liddicoat P V et al. *Nat. Commun.* **1** 63 (2010)
49. Sauvage X et al. *Adv. Eng. Mater.* **17** 1821 (2015)
50. Popov A G et al., in *Struktura i Svoistva Nanokristallicheskikh Materialov* (Structure and Properties of Nanocrystalline Materials) (Exec. Eds G G Taluts, N I Noskova) (Yekaterinburg: UrO RAN, 1999) p. 245
51. Burgio N et al. *Nuovo Cimento D* **13** 459 (1991)
52. Rodríguez Torres C E, Sánches F H, Mendoza Zélis L A *Phys. Rev. B* **51** 12142 (1995)
53. Sherif El-Eskandarany M et al. *Appl. Phys. Lett.* **70** 1679 (1997)
54. Tsurin V A, Barinov V A, Pupyshev S B *Tech. Phys. Lett.* **21** 449 (1995); *Pis'ma Zh. Tekh. Fiz.* **21** (12) 20 (1995)
55. Politis C *Int. J. Mod. Phys. B* **22** 2905 (2008)
56. Suryanarayana C, Inoue A *Bulk Metallic Glasses* (Boca Raton, FL: CRC Press, 2011)
57. Descamps M, Willart J F *Adv. Drug Deliv. Rev.* **100** 51 (2016)
58. Bellon P, Averback R S *Phys. Rev. Lett.* **74** 1819 (1995)
59. Shtremel M A *Met. Sci. Heat Treat.* **44** 324 (2002); *Metalloved. Term. Obrabotka Met.* **8** (8) 10 (2002)
60. Lyubov B Ya, Shmakov V A *Fiz. Met. Metalloved.* **29** 968 (1970)
61. Lyubov B Ya *Diffuzionnye Protsessy v Neodnorodnykh Tverdykh Sredakh* (Diffusion Processes in Nonuniform Solid Media) (Moscow: Nauka, 1981)
62. Teitel' E I et al. *Phys. Met. Metallogr.* **113** 1162 (2012); *Fiz. Met. Metalloved.* **113** 1230 (2012)
63. Ermakov A E et al. *Phys. Met. Metallogr.* **88** 211 (1999); *Fiz. Met. Metalloved.* **88** (3) 5 (1999)
64. Rybin V V *Bol'shie Plasticheskie Deformatsii i Razrushenie Metallov* (Severe Plastic Deformations and Fracturing of Metals) (Moscow: Metallurgiya, 1986)
65. Glezer A M, Metlov L S *Phys. Solid State* **52** 1162 (2010); *Fiz. Tverd. Tela* **52** 1090 (2010)
66. Lejček P *Grain Boundary Segregation in Metals* (Springer Series in Materials Science, Vol. 136) (Berlin: Springer-Verlag, 2010)
67. Sutton A P, Balluffi R W *Interfaces in Crystalline Materials* (Oxford: Clarendon Press, 1995)
68. Skakov Yu A *Met. Sci. Heat Treat.* **47** 296 (2005); *Metalloved. Term. Obrabotka Met.* (7) 45 (2005)
69. Shtremel' M A *Met. Sci. Heat Treat.* **46** 146 (2004); *Metalloved. Term. Obrabotka Met.* (4) 12 (2004)
70. Korznikova E et al., in *Ultrafine Grained Materials IV* (Eds Y T Zhu et al.) (Warrendale, PA: The Minerals, Metals and Materials Soc., TMS, 2006) p. 97
71. Ungár T et al. *Mater. Sci. Eng. A* **462** 398 (2007)
72. Dorofeev G A et al. *Mater. Sci. Forum* **343–346** 585 (2000)
73. Kilmametov A R et al. *Mater. Sci. Eng. A* **503** 10 (2009)
74. Lotkov A I et al. *Phys. Mesomech.* **10** 179 (2007); *Fiz. Mezomekh.* **10** (3) 67 (2007)
75. Straumal B B et al. *Mater. Lett.* **145** 63 (2015)
76. Straumal B B et al. *Mater. Lett.* **161** 735 (2015)
77. Borchers C et al. *Acta Mater.* **97** 207 (2015)
78. Lee S, Horita Z *Mater. Trans.* **53** 38 (2012)
79. Edalati K et al. *Scr. Mater.* **66** 386 (2012)
80. Cubero-Sesin J M, Horita Z *Mater. Trans.* **53** 46 (2012)
81. Mazilkin A A et al. *Phys. Solid State* **49** 868 (2007); *Fiz. Tverd. Tela* **49** 824 (2007)
82. Straumal B B et al. *J. Mater. Sci.* **46** 4243 (2011)
83. Edalati K et al. *Mater. Trans.* **57** 533 (2016)
84. Edalati K et al. *Mater. Sci. Eng. A* **714** 167 (2018)
85. Straumal B B et al. *Int. J. Mater. Res.* **106** 657 (2015)
86. Edalati K, Horita Z *Acta Mater.* **59** 6831 (2011)
87. Straumal B B et al. *Mater. Trans.* **53** 63 (2012)
88. Edalati K et al. *Mater. Sci. Eng. A* **559** 506 (2013)
89. Mazilkin A A et al. *Def. Diff. Forum* **237–240** 739 (2005)
90. Mazilkin A A et al. *Def. Diff. Forum* **249** 155 (2006)
91. Kulagin R et al. *Mater. Lett.* **222** 172 (2018)
92. Kral P et al. *Mater. Sci. Eng. A* **723** 287 (2018)
93. Sabbaghianrad S, Torbati-Sarraf S A, Langdon T G *Mater. Sci. Eng. A* **712** 373 (2018)
94. Tirsatine K et al. *J. Alloys Comp.* **753** 46 (2018)
95. Alawadhi M Y et al. *J. Mater. Res. Technol.* **6** 369 (2017)
96. Azabou M et al. *Int. J. Adv. Manuf. Technol.* **87** 981 (2016)
97. Mazilkin A A et al. *Acta Mater.* **54** 3933 (2006)
98. Straumal B B et al. *Mater. Lett.* **118** 111 (2014)
99. Huang Y et al. *Mater. Sci. Eng. A* **656** 55 (2016)
100. Lugo N et al. *Mater. Sci. Eng. A* **477** 366 (2008)
101. Čížek J et al. *Acta Mater.* **59** 2322 (2011)
102. Liao X Z et al. *J. Appl. Phys.* **96** 636 (2004)
103. Shamsborhan M, Ebrahimi M *J. Alloys Comp.* **682** 552 (2016)
104. Tang C, Li H, Li S *Trans. Nonferr. Met. Soc. China* **26** 1736 (2016)
105. Mao Z N et al. *Mater. Sci. Eng. A* **674** 186 (2016)
106. Bagherpour E et al. *Mater. Sci. Eng. A* **674** 221 (2016)
107. Bagherpour E et al. *Mater. Sci. Eng. A* **666** 324 (2016)
108. Yadav P C et al. *J. Mater. Eng. Perform.* **25** 2604 (2016)
109. Xu C, Horita Z, Langdon T G *Mater. Sci. Eng. A* **528** 6059 (2011)
110. Edalati K, Horita Z *Mater. Sci. Eng. A* **528** 7514 (2011)
111. Korznikov A V et al. *Nanostruct. Mater.* **4** 159 (1994)
112. Ivanisenko Yu et al. *Acta Mater.* **51** 5555 (2003)
113. Ivanisenko Yu et al. *Scripta Mater.* **49** 947 (2003)
114. Zrnik J et al. *J. Mater. Sci.* **45** 4822 (2010)
115. Bayramoglu S et al. *Mater. Sci. Eng. A* **527** 927 (2010)
116. Ning J et al. *Mater. Sci. Eng. A* **581** 8 (2013)
117. Todaka Y et al. *Mater. Sci. Forum* **584–586** 597 (2008)
118. Liao X Z et al. *Appl. Phys. Lett.* **88** 021909 (2006)
119. Pippan R et al. *Annu. Rev. Mater. Res.* **40** 319 (2010)
120. Edalati K et al. *Acta Mater.* **69** 68 (2014)
121. Tejedor R et al. *Mater. Sci. Eng. A* **743** 597 (2019)
122. Mohamed I F et al. *Mater. Sci. Eng. A* **704** 112 (2017)
123. Edalati K et al. *Int. J. Hydrog. Energy* **41** 8917 (2016)
124. Isik M et al. *J. Mech. Behav. Biomed. Mater.* **59** 226 (2016)

125. Isik M et al. *Mater. Trans.* **57** 1109 (2016)
126. Hongo T et al. *Mater. Sci. Eng. A* **618** 1 (2014)
127. Edalati K et al. *Mater. Trans.* **53** 123 (2012)
128. Hanna A et al. *J. Alloys Comp.* **778** 61 (2019)
129. Bourezg Y I et al. *Mater. Sci. Eng. A* **724** 477 (2018)
130. Bazarnik P et al. *Mater. Sci. Eng. A* **712** 513 (2018)
131. Cardona D M M et al. *J. Mater. Res. Technol.* **6** 355 (2017)
132. Torbati-Sarraf S A et al. *J. Alloys Comp.* **712** 185 (2017)
133. Koch C C, Langdon T G, Lavernia E J *Metall. Mater. Trans. A* **48** 5181 (2017)
134. Mazilkin A A et al. *Mater. Lett.* **84** 63 (2012)
135. Straumal B B et al. *Acta Mater.* **52** 4469 (2004)
136. Ito Y, Edalati K, Horita Z *Mater. Sci. Eng. A* **679** 428 (2017)
137. Johnson W L *Prog. Mater. Sci.* **30** 81 (1986)
138. Cahn R W, in *Materials Science and Technology*: *A Comprehensive Treatment* (Eds R W Cahn, P Haasen, E J Kramer) Vol. 9 *Glasses and Amorphous Materials* (Ed. J Zarzycki) (Weinheim: Wiley-VCH, 1991) p. 493
139. Bouhki M, Bruson A, Guilmin P *Solid State Commun.* **79** 389 (1991)
140. de Boer F R et al. *Cohesion in Metals*: *Transition Metal Alloys* (Cohesion and Structure, Vol. 1) (Amsterdam: North-Holland, 1988)
141. Frenkel Ya I *Vvedenie v Teoriyu Metallov* (Introduction to the Theory of Metals) (Leningrad: Nauka, 1972)
142. Glezer A M, Molotilov B V *Phys. Met. Metallogr.* **69** (2) 1 (1990); *Fiz. Met. Metalloved.* **69** (2) 5 (1990)
143. Glezer A M *Ross. Khim. Zh.* **46** (5) 57 (2002)
144. Gutkin M Yu, Ovid'ko I A *Plastic Deformation in Nanocrystalline Materials* (Berlin: Springer, 2004)
145. Dobromyslov A V et al. *Materialovedenie* (10) 43 (2001)
146. Blank V D, Estrin E I *Phase Transitions in Solids under High Pressure* (Boca Raton, FL: CRC Press, 2014); Translated from Russian: *Fazovye Prevrashchenia Tverdykh Tel pri Vysokom Davlenii* (Moscow: Fizmatlit, 2011)
147. Morris R C *J. Appl. Phys.* **50** 3250 (1979)
148. Tat'yanin E V et al. *Phys. Solid State* **39** 1097 (1997); *Fiz. Tverd. Tela* **39** 1237 (1997)
149. Martin G *Phys. Rev. B* **30** 1424 (1984)
150. Bellon P, Martin G *Phys. Rev. B* **39** 2403 (1989)
151. Straumal B B et al. *Mater. Trans.* **53** 63 (2012)
152. Straumal B B et al. *High Temp. Mater. Process.* **31** 339 (2012)
153. Pochet P et al. *Phys. Rev. B* **52** 4006 (1995)
154. Prokoshkin S D et al. *Acta Mater.* **53** 2703 (2005)
155. Razumov I K, Gornostyrev Yu N, Ermakov A E *Phys. Solid State* **61** 214 (2019); *Fiz. Tverd. Tela* **61** 346 (2019)
156. Pavlov V A *Phys. Met. Metallogr.* **67** (5) 90 (1989); *Fiz. Met. Metalloved.* **67** 924 (1989)
157. Popov A G et al. *Phys. Met. Metallogr.* **104** 238 (2007); *Fiz. Met. Metalloved.* **104** 251 (2007)
158. Gaviko V S et al.*Phys. Met. Metallogr.* **92** 158 (2001); *Fiz. Met. Metalloved.* **92** (2) 58 (2001)
159. Metlov L S *Phys. Rev. Lett.* **106** 165506 (2011)
160. Gapontsev V L, Koloskov V M *Met. Sci. Heat Treat.* **49** 503 (2007); *Metalloved. Term. Obrabotka Met.* (11) 3 (2007)
161. Lam N Q, Okamoto P R, Jonson R A *J. Nucl. Mater.* **78** 408 (1978)
162. Wolfer W G *J. Nucl. Mater.* **114** 292 (1983)
163. Ovid'ko I A, Reizis A B *Phys. Solid State* **45** 1679 (2003); *Fiz. Tverd. Tela* **45** 1600 (2003)
164. Ovid'ko I A, Sheinerman A G *Appl. Phys. A* **81** 1083 (2005)
165. Mazilkin A A et al. *J. Mater. Sci.* **46** 4336 (2011)
166. Shingu P H (Ed.) 'Mechanical alloying' *Mater. Sci. Forum* **88 – 90** (1992) https://doi.org/10.4028/www.scientific.net/MSF.88-90
167. Yelsukov E P, Dorofeev G A *J. Mater. Sci.* **39** 5071 (2004)
168. González G et al. *Mater. Sci. Forum* **386–388** 159 (2002)
169. Uenishi K et al. *Z. Metallkund.* **83** 132 (1992)
170. Wanderka N et al. *Ultramicroscopy* **89** 189 (2001)
171. Cherdyntsev V V, Kaloshkin S D *Phys. Met. Metallogr.* **109** 492 (2010); *Fiz. Met. Metalloved.* **109** 529 (2010)
172. Qi M, Zhu M, Yang D Z *J. Mater. Sci. Lett.* **13** 966 (1994)
173. Sauvage X, Wetscher F, Pareige P *Acta Mater.* **53** 2127 (2005)
174. Quelennec X et al. *Philos. Mag.* **90** 1179 (2010)
175. Bachmaier A et al. *Acta Mater.* **60** 860 (2012)
176. Dorofeev G A, Elsukov E P *Phys. Met. Metallogr.* **103** 593 (2007); *Fiz. Met. Metalloved.* **103** 626 (2007)
177. Yelsukov E P et al. *Mater. Sci. Forum* **269–272** 151 (1998)
178. Hightower A, Fultz B, Bowman R C (Jr.) *J. Alloys Comp.* **252** 238 (1997)
179. Elsukov E P et al. *Khim. Interesakh Ustoichivogo Razvitiya* **13** 191 (2005)
180. Uenishi K et al. *Mater. Sci. Eng. A* **134** 1342 (1991)
181. Delogu F et al. *Philos. Mag. B* **76** 651 (1997)
182. Pilyugin V P et al. *Bull. Russ. Acad. Sci. Phys.* **78** 988 (2014); *Izv. Ross. Akad. Nauk Ser. Fiz.* **78** 1238 (2014)
183. Baricco M et al. *Philos. Mag. B* **68** 957 (1993)
184. Gente C, Oehring M, Bormann R *Phys. Rev. B* **48** 13244 (1993)
185. Czubayko U et al. *Mater. Sci. Eng. A* **327** 54 (2002)
186. Cherdyntsev V V et al. *Phys. Met. Metall.* **97** 392 (2004); *Fiz. Met. Metalloved.* **97** (4) 71 (2004)
187. Hahn J D, Wu F, Bellon P *Metall. Mater. Trans. A* **35** 1105 (2004)
188. Veltl G, Scholz B, Kunze H-D *Mater. Sci. Eng. A* **134** 1410 (1991)
189. Kuyama J et al. *Jpn. J. Appl. Phys.* **30** L854 (1991)
190. Xu J et al. *J. Appl. Phys.* **79** 3935 (1996)
191. Freundenberger J, Botcharova E, Schultz L *J. Mater. Sci.* **39** 5343 (2004)
192. Shabashov V A et al. *Mater. Sci. Eng. A* **346** 196 (2003)
193. Languillaume J, Kapelski G, Baudelet B *Acta Mater.* **45** 1201 (1997)
194. Zhou L et al. *Acta Mater.* **56** 78 (2008)
195. Sitdikov V D et al. *Rev. Adv. Mater. Sci.* **47** 59 (2016)
196. Korneva A et al. *Inżynieria Materialowa* **34** 306 (2013)
197. Straumal B B et al. *Mater. Lett.* **98** 217 (2013)
198. von Bertalanffy L *Science* **111** 23 (1950)
199. Straumal B B et al. *JETP Lett.* **100** 376 (2014); *Pis'ma Zh. Eksp. Teor. Fiz.* **100** 418 (2014)
200. Korneva A et al. *Mater. Lett.* **179** 12 (2016)
201. Korneva A et al. *Mater. Charact.* **118** 411 (2016)
202. Korneva A et al. *IOP Conf. Ser. Mater. Sci. Eng.* **63** 012093 (2014)
203. Straumal B B et al. *Mater. Lett.* **138** 255 (2015)
204. Korneva A et al. *Mater. Charact.* **114** 151 (2016)
205. Straumal B B et al. *Acta Mater.* **122** 60 (2017)
206. Korneva A et al. *Materials* **12** 447 (2019)
207. Straumal B B et al. *Int. J. Mater. Res.* **110** 608 (2019)
208. López G A et al. *Mater. Today Proc.* **2** (Suppl. 3) S747 (2015)
209. Straumal B B et al. *Acta Mater.* **125** 274 (2017)
210. Gusev A A *Sib. Khim. Zh.* (2) 135 (1993)
211. Tian H H, Atzmon M *Mater. Sci. Forum* **343–346** 284 (2000)
212. Ma E et al. *Mater. Sci. Eng. A* **286** 48 (2000)
213. Odunuga S et al. *Phys. Rev. Lett.* **95** 045901 (2005)
214. Razumov I K *Russ. J. Phys. Chem. A* **84** 1485 (2010); *Zh. Fiz. Khim.* **84** 1632(2010)
215. Lifshitz E M, Pitaevskii L P *Physical Kinetics* (Oxford: Pergamon Press, 1981); Translated from Russian: *Fizicheskaya Kinetika* (Moscow: Nauka, 1979)
216. Perez M et al. *Philos. Mag.* **85** 2197 (2005)
217. Lund A C, Schuh C A *Acta Mater.* **52** 2123 (2004)
218. Gleiter H *Acta Metall.* **16** 455 (1968)
219. Gutkin M Yu, Ovid'ko I A *Defekty i Mekhanizmy Plastichnosti v Nanokristallicheskikh i Nekristallicheskikh Materialakh* (Defects and Plasticity Mechanisms in Nanocrystalline and Non-Crystalline Materials) (St. Petersburg: Yanus, 2001)
220. Pozdnyakov V A, Glezer A M *Phys. Solid State* **44** 732 (2002); *Fiz. Tver. Tela* **44** 705 (2002)
221. Voronova L M, Shashchukhina T I, Degtyarev M V *Deform. Rasrushenie Mater.* (7) 20 (2008)
222. Voronova L M et al. *Deform. Rasrushenie Mater.* (3) 9 (2011)
223. Chashchukhina T I et al. *Phys. Met. Metallogr.* **111** 304 (2011); *Fiz. Met. Metalloved.* **111** 3315 (2011)
224. Skakov Yu A *Mater. Sci. Forum* **343–346** 597 (2000)
225. Skakov Yu A *Met. Sci. Heat Treat.* **46** 137 (2004); *Metalloved. Term. Obrabotka Met.* (4) 3 (2004)
226. Noskovich O I et al. *Acta Metall. Mater.* **39** 3091 (1991)
227. Razumov I K *Kondens. Sredy Mezhfaznye Granitsy* **12** 394 (2010)
228. Karkina L E et al. *Comput. Mater. Sci.* **112** 18 (2016)
229. Cottrell A H, Jaswon M A *Proc. R. Soc. Lond. A* **199** 104 (1949)
230. Rakin V G, Buinov N N *Fiz. Met. Metalloved.* **11** (1) 59 (1961)
231. Shabashov V A et al. *Metallofizika* **12** (4) 107 (1990)

232. McGrath J T, Bratina W J *Acta Metall.* **15** 329 (1967)
233. Chang L, Barnard S J, Smith G DW, in *Fundamentals of Aging and Tempering in Bainitic and Martensitic Steel Products. Gilbert R. Speich Symp. Proc., an Intern. Symp. at the 34th Mechanical Working and Steel Processing Conf., Montreal, Quebec, Canada, October 25 – 28, 1992* (Ed G Krauss, P E Repes) (Warrendale, PA: Iron and Steel Society, 1992) p. 19
234. Jayaram R, Miller M K *Scripta Metall. Mater.* **33** 19 (1995)
235. Blavette D et al. *Science* **286** 2317 (1999)
236. Kuzmina M et al. *Science* **349** 1080 (2015)
237. Sagaradze V V et al. *Phys. Met. Metallogr.* **116** 1002 (2015); *Fiz. Met. Metalloved.* **116** 1056 (2015)
238. Sagaradze V V et al. *Philos. Mag.* **96** 1724 (2016)
239. Doherty R D *Metal Sci.* **16** 1 (1982)
240. Octor H, Naka S *Philos. Mag. Lett.* **59** 229 (1989)
241. Naka S et al. *Scripta Metall.* **23** 501 (1989)
242. Gupta S P *Solid State Phase Transformation* (New Delhi: Allied Publ. (P) Ltd, 2002)
243. Sallez N et al. *J. Nucl. Mater.* **472** 118 (2016)
244. Jiang J Z, Gente C, Bormann R *Mater. Sci. Eng. A* **242** 268 (1998)
245. Bouchaud E, Naka S, Octor H *J. Phys. Colloq.* **51** C1-451 (1990)
246. Cahn J W *Acta Metall.* **10** 789 (1962)
247. Lücke K, Stüwe H P *Acta Metall.* **19** 1087 (1971)
248. Takeshita T *J. Alloys Comp.* **193** 231 (1993)
249. Yermakov A Ye *Mater. Sci. Forum* **179 – 181** 455 (1995)
250. Gong W, Hadjipanayis G C, Krause R F *J. Appl. Phys.* **75** 6649 (1994)
251. Barinov V A et al. *Phys. Status Solidi A* **123** 527 (1991)
252. Abrosimova G E et al. *Phys. Solid State* **49** 1034 (2007); *Fiz. Tverd. Tela* **49** 983 (2007)
253. Prigogine I *Introduction to Thermodynamics of Irreversible Processes* (Springfield, IL: Thomas, 1955); Translated into Russian: *Vvedenie v Termodinaiku Neobratimykh Protsessov* (Moscow–Izhevsk: RKhD, 2001)
254. Nicolis G, Prigogine I *Self-Organization in Nonequilibrium Systems: from Dissipative Structures to Order through Fluctuations* (New York: Wiley, 1977)
255. Zhabotinskii A M *Kontsentratsionnye Kolebaniya* (Concentration Oscillations) (Moscow: Nauka, 1974)
256. Sherif El-Eskandarany M et al. *Acta Metall.* **50** 1113 (2002)
257. Seah M P, Sanz J M, Hofmann S *Thin Solid Films* **81** 239 (1981)
258. Seah M P, Hondros E D *Proc. R. Soc. Lond. A* **335** 191 (1973)
259. McLean D *Grain Boundaries in Metals* (London: Oxford Univ. Press, 1957); Translated into Russian: *Granitsy Zeren v Metallakh* (Moscow: Metallurgizdat, 1960)
260. Bokstein B, Balandina N (Eds) "Grain boundary diffusion and grain boundary segregation" *Defect Diffus. Forum* **156** (1998) https://doi.org/10.4028/www.scientific.net/DDF.156
261. Raabe D et al. *Acta Mater.* **61** 6132 (2013)
262. Kirchheim R *Acta Mater.* **50** 413 (2002)
263. Chookajorn T, Murdoch H A, Schuh C A *Science* **337** 951 (2012)
264. Sauvage X et al. *Mater. Sci. Eng. A* **540** 1 (2012)
265. Peng L et al. *Phys. Chem. Chem. Phys.* **17** 27940 (2015)
266. Ringe E, Van Duyne R P, Marks L D *Nano Lett.* **11** 3399 (2011)
267. Yan Z et al. *Nano Lett.* **18** 2696 (2018)
268. Fowler R H, Guggenheim E A *Statistical Thermodynamics; a Version of Statistical Mechanics for Students of Physics and Chemistry* (Cambridge: The Univ. Press, 1939)
269. Ishida K *J. Alloys Comp.* **235** 244 (1996)
270. Slezov V V, Davydov L N, Rogozhkin V V *Phys. Solid State* **37** 1964 (1995); *Fiz. Tverd. Tela* **37** 3565 (1995)
271. Razumov I K *Russ. J. Phys. Chem. A* **88** 494 (2014); *Zh. Fiz. Khim.* **88** 458 (2014)
272. Razumov I K *Russ. J. Phys. Chem.* **92** 1338 (2018); *Zh. Fiz. Khim.* **92** 1098 (2018)
273. Guttmann M *Surf. Sci.* **53** 213 (1975)
274. Fel'dman E P, Yurchenko V M, Mel'nik T N *Metallofiz. Noveishie Tekhnol.* **22** (1) 60 (2000)
275. Zheng L, Xu T *Metall. Mater. Trans. A* **36** 3311 (2005)
276. Wang M Q, Wang K, Deng Q *Mater. Sci. Technol.* **25** 1238 (2009)
277. Weissmüller J *Nanostruct. Mater.* **3** 261 (1993)
278. Darling K A et al. *Scripta Mater.* **59** 530 (2008)
279. Botcharova E, Freudenberger J, Schulz L *Acta Mater.* **54** 3333 (2006)
280. Millett P C, Selvam R P, Saxena A *Acta Mater* **55** 2329 (2007)
281. Cserháti Cs, Szabó I A, Beke D L *J. Appl. Phys.* **83** 3021 (1998)
282. Beke D L, Cserháti C, Szabó I A *J. Appl. Phys.* **95** 4996 (2004)
283. Trelewicz J R, Schuh C A *Phys. Rev. B* **79** 094112 (2009)
284. Cahn J W, Hilliard J E *J. Chem. Phys.* **28** 258 (1958)
285. Gouyet J-F et al. *Adv. Phys.* **52** 523 (2003)
286. Gornostyrev Yu N, Razumov I K, Yermakov A Ye *J. Mater. Sci.* **39** 5003 (2004)
287. Razumov I K, Gornostyrev Yu N, Yermakov A Ye *J. Alloys Compound* **434 – 435** 535 (2007)
288. Razumov I K, Gornostyrev Yu N, Yermakov A Ye *Rev. Adv. Mater. Sci.* **18** 767 (2008)
289. Kar'kin I N et al. *Phys. Solid State* **59** 106 (2017); *Fiz. Tverd. Tela* **59** (1) 103 (2017)
290. Löffler J, Weissmüller J *Phys. Rev. B* **52** 7076 (1995)
291. Frase H N et al. *Philos. Mag. B* **80** 1545 (2000)
292. Straumal B B et al. *Mater. Lett.* **159** 432 (2015)
293. Gleiter H *Nanostruct. Mater.* **6** 3 (1995)
294. Wunderlich W, Ishida Y, Maurer R *Scripta Metall. Mater.* **24** 403 (1990)
295. Valiev R Z, Islamgaliev R K *Phys. Met. Metallogr.* **85** 367 (1998); *Fiz. Met. Metalloved.* **85** (3) 161 (1998)
296. Islamgaliev R K, Valiev R Z *Phys. Met. Metallogr.* **87** 215 (1999); *Fiz. Met. Metalloved.* **87** (3) 46 (1999)
297. Straumal B B et al. *Acta Mater.* **52** 4469 (2004)
298. Razumov I K et al. *Phys. Met. Metallogr.* **96** 351 (2003); *Fiz. Met. Metalloved.* **96** (4) 5 (2003)
299. Gapontsev V L et al. *Phys. Met. Metallogr.* **99** 365 (2005); *Fiz. Met. Metalloved.* **99** (4) 26 (2005)
300. Starikov S A et al. *Diagn. Resour. Mech. Mater. Struct.* (6) 48 (2016)
301. Bernshtein M L et al. *Metallovedenie i Termicheskaya Obrabotka Stali i Chuguna* (Metallurgy and Heat Treatment of Steel and Cast Iron) Vol. 2 *Stroenie Stali i Chuguna* (Structure of Steel and Cast Iron) (Moscow: Intermet Engineering, 2005)
302. Yang C-W, Williams D B, Goldstein J I *J. Phase Equilib.* **17** 522 (1996)
303. Shah L H, Gerlich A, Zhou Y *Int. J. Adv. Manufact. Technol.* **94** 2667 (2018)
304. Fallah V et al. *Acta Mater.* **82** 457 (2015)
305. Kuzmina M, Ponge D, Raabe D *Acta Mater.* **86** 182 (2015)
306. Mirzoev A A, Mirzaev D A, Yalolov M M, in *Proc. of the World Congress on Engineering, WCE 2009, July 1 – 3, 2009, London, U.K.* Vol. 1 (Eds S I Ao et al.) (London: Newswood Ltd, 2009)
307. Yermakov A Ye et al. *Mater. Sci. Forum* **343–346** 577 (2000)
308. Nechaev Yu S et al. *Phys. Met. Metallogr.* **60** (3) 116 (1985); *Fiz. Met. Metalloved.* **60** 542(1985)
309. Kinoshita C, Eguchi T *Acta Metall.* **20** 45 (1972)
310. Agullo-Lopez F, Catlow C R A, Townsend P D *Point Defects in Materials* (London: Academic Press, 1988)
311. Shtremel' M A *Met. Sci. Heat Treat.* **49** 517 (2007); *Metalloved. Term. Obrabotka Met.* (11) 18 (2007)
312. Eckert J et al. *J. Appl. Phys.* **73** 2794 (1993)
313. Popov V V, Sergeev A V *Phys. Met. Metallogr.* **118** 1091 (2017); *Fiz. Met. Metalloved.* **118** 1149 (2017)
314. Bekker H et al. (Eds) *Diffusion in Solids Metals and Alloys* (Landolt-Börnstein New Series Vol. III/26) (Berlin: Springer-Verlag, 1990)
315. Butrymowicz D B, Manning J R, Read M E *J. Phys. Chem. Ref. Data* **2** 643 (1973)
316. Ribbe J, Schmitz G, Divinski S V *Def. Diff. Forum.* **289 – 292** 211 (2009)
317. Butrymowicz D B, Manning J R, Read M E *J. Phys. Chem. Ref. Data* **5** 103 (1976)
318. Herzig C, Divinski S V *Mater. Trans.* **44** 14 (2003)
319. Schafler E et al. *Mater. Sci. Eng. A* **410 – 411** 169 (2005)
320. Hosford W F *Physical Metallurgy* (Boca Raton, FL: Taylor and Francis, 2005)
321. Skakov Yu A *Met. Sci. Heat Treat.* **49** 514 (2007); *Metalloved. Term. Obrabotka Met.* (11) 15 (2007)
322. Indenbom V L *JETP Lett.* **12** 369 (1970); *Pis'ma Zh. Eksp. Teor. Fiz.* **12** 526 (1970)
323. Indenbom V L, Orlov A N *Fiz. Met. Metalloved.* **43** 469 (1977)

324. Rozhanskii V N et al. *Deformatsionnoe Uprochnenie* (Deformation Strengthening) (Kharkiv: Izd. FTINT AN USSR, 1969)
325. Gertsriken D S, Mazanko V F, Fal'chenko V M *Metallofizika* **5** (4) 74 (1983)
326. Saralidze Z K, Galustashvili M V, Driaev D G *Phys. Solid State* **48** 1298 (2006); *Fiz. Tverd. Tela* **48** 1229 (2006)
327. Sørensen M R, Mishin Yu, Voter A F *Phys. Rev. B* **62** 3658 (2000)
328. Razumov I K, Gornostyrev Yu N, Ermakov A E *Phys. Met. Metalogr.* **119** 1133 (2018); *Fiz. Met. Metalloved.* **119** 1195 (2018)
329. Rybin V V, Zolotorevskiy N Yu, Zhukovskiy I M *Phys. Met. Metallogr.* **69** (1) 1 (1990); *Fiz. Met. Metalloved.* **69** (1) 5 (1990)
330. Sarafanov G F, Perevezentsev V N *Tech. Phys. Lett.* **33** 400 (2007); *Pis'ma v Zh. Tekh. Fiz.* **33** (9) 87 (2007)
331. Shabashov V A et al. *Phys. Met. Metallogr.* **117** 805 (2016); *Fiz. Met. Metalloved.* **117** 833 (2016)
332. Popov L E, Kozlov E V *Mekhanicheskie Svoistva Uporyadochennykh Tverdykh Rastvorov* (Mechanical Properties of Ordered Solid Solutions) (Moscow: Metallurgiya, 1970)
333. Koch C C *Rev. Adv. Mater. Sci.* **5** (2) 91 (2003)
334. Le Caër G, Begin-Colin S, Delcroix P, in *Materials Research in Atomic Scale by Mössbauer Spectroscopy* (NATO Science Ser., Ser. II, Vol. 94, Eds M Mashlan, M Miglierini, P Schaaf) (Dordrecht: Springe, 2003) p. 11
335. Volkov V A et al. *Phys. Met. Metallogr.* **117** 178 (2016); *Fiz. Met. Metalloved.* **117** 186 (2016)
336. Barinov V A et al. *Phys. Met. Metallogr.* **74** 412 (1992); *Fiz. Met. Metalloved.* **10** (4) 148 (1992)
337. Tsurin V A, Barinov V A *Tech. Phys. Lett.* **24** 556 (1998); *Pis'ma Zh. Tekh. Fiz.* **24** (14) 35 (1998)
338. Shangurov A V et al. *Fiz. Met. Metalloved.* **61** 884 (1986)
339. Teytel Ye I et al. *Phys. Met. Metallogr.* **70** (1) 88 (1990); *Fiz. Met. Metalloved.* (7) 195 (1990)
340. Teytel' Ye L et al. *Phys. Met. Metallogr.* **70** (2) 74 (1990); *Fiz. Met. Metalloved.* (8) 83 (1990)